Advanced Fiber Materials (2023) 5:868–895
https://doi.org/10.1007/s42765-022-00254-4

REVIEW

Fiber-Shaped Soft Actuators: Fabrication, Actuation Mechanism and Application

Yue Yu[3] · Juanjuan Wang[1] · Xue Han[1] · Shuguang Yang[2] · Gaihong An[4] · Conghua Lu[1,3]

Received: 3 September 2022 / Accepted: 26 December 2022 / Published online: 20 February 2023

Abstract

As mechanical devices for moving or controlling mechanisms or systems, actuators have attracted increasing attention in various fields. Compared to traditional actuators with rigid structures, soft actuators made up of stimulus-responsive soft materials are more adaptable to complex working conditions due to soft bodies and diverse control styles. Different from plate-shaped soft actuators, which have the limited deformations between two dimensional (2D) and 3D-configurations such as bending and twisting, fiber-shaped soft actuators (FSAs) own intriguing deformation modes to satisfy diverse practical applications. In this mini review, the recent progress on the controlled fabrication of the FSAs is presented. The advantages and disadvantages of each fabrication method are also demonstrated. Subsequently, the as-developed actuation mechanisms of the FSAs are displayed. Additionally, typical examples of the related applications of the FSAs in different fields have been discussed. Finally, an outlook on the development tendency of the FSAs is put forward as well.

Keywords Soft actuator · Actuation mechanism · Fiber-shaped structure · Smart materials

Introduction

With the rapid progress of science and technology, the emerging wide applications of actuators in various fields have been helping people to deal with complex and tedious working conditions, such as excessive loading, repetitive processing and dangerous tasks. However, traditional actuators based on rigid structures have limited the practical applications especially in narrow and changeable environments due to the internal shortcomings (e.g., a limited freedom degree and a relatively complex controlling/sensing system with intricate circuits). To address these challenges, in recent decades, a number of efforts have been made to develop a novel generation of soft actuations (SAs) composed of soft materials. Hereinto, the initial soft actuators that are controlled by touch methods mainly concern fluidic actuation and mechanical actuation, and they are usually connected with external driving devices [1–4]. Subsequently, a wide range of interesting SAs based on stimulus-responsive smart materials have been rapidly developed. The involved typical smart materials include hydrogels [5, 6], shape-memory polymers [7, 8], liquid crystal polymers [9], dielectric elastomers [10], and carbon-based materials [11]. Under external stimuli, these smart soft materials have obvious deformability [12, 13], endowing the corresponding SAs with excellent adaptability to complicated tasks, narrow space and ever-changing working situations [14, 15].

In the initial period, soft actuators are employed mainly based on bulk and plate-shaped structures, which show an in-plane deformation in the case of the change in the volume, alignment and arrangement [16]. Afterwards, a great

✉ Shuguang Yang
shgyang@dhu.edu.cn

✉ Gaihong An
angaihong@163.com

✉ Conghua Lu
chlu@tju.edu.cn

1 School of Materials Science and Engineering, Tianjin Key Laboratory of Building Green Functional Materials, Tianjin Chengjian University, Tianjin 300384, People's Republic of China

2 State Key Laboratory for Modification of Chemical Fibers and Polymer Materials, Center for Advanced Low-Dimension Materials, College of Materials Science and Engineering, Donghua University, Shanghai 201620, China

3 School of Materials Science and Engineering, Tianjin University, Tianjin 300072, People's Republic of China

4 Environmental and Operational Medicine Research Department, Military Medical Sciences Academy, Tianjin 300050, People's Republic of China

number of investigations focus on the soft actuators with bimorph or gradient structures, in which reversible deformations between two dimensional (2D) shapes and three dimensional (3D) ones are involved. In this case, however, limited deformation modes such as bending [17] and twisting [18] are available. By contrast, one dimension (1D)-shaped soft actuators with various fine and complex locomotions can be easily accessible owing to the outstanding flexibility and anisotropic character of the 1D shape. In nature, many living creatures have used these 1D-shaped structures to adapt to the change of environments/circumstances. Typically, animals, especially mammal, perform diverse body motions by controlling the contraction or relaxation of the attached muscles on the skeleton or other organs; the stem of sunflower exhibits phototropic bending towards sunshine direction to harvest more energy. These natural phenomena have inspired people to develop novel fiber-shaped soft actuators (FSAs). The introduction of smart materials further endows the 1D-shaped FSAs with more abundant actuation performances and applications in a new way. It is noted that with the rapid development of the fabrication technology, many FSAs based on common materials that have weak or even no stimulus-responsive ability can also exhibit responsiveness [19–22]. Furthermore, thanks to the compatibility of the FSAs with various structures, the FSAs can be well integrated with other functional components to generate diverse advanced FSA-based smart devices [23, 24].

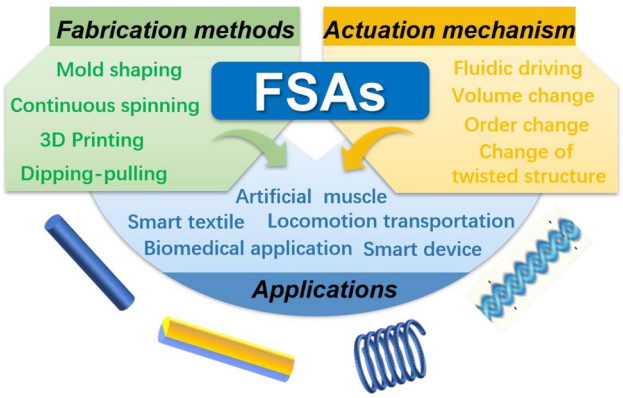

Fig. 1 Schematic illustration of the fabrication methods, actuation mechanism and the applications for the FSAs

In this review, the recent progress of the FSAs will be reported (Fig. 1). According to the mechanical or physical properties of raw materials, different methods have been proposed to fabricate the FSAs with well-designed structures for the desirable actuation ability. Thus, in the first part, the typical fabrication methods are summarized. Notably, the advantages and disadvantages of each method are displayed. The actuation mechanisms corresponding to typical raw materials and structures are discussed in the following part. Meanwhile, actuation styles and specific properties of the FSAs in the recently reported works are also demonstrated. Subsequently, typical examples of the applications of the FSAs are also displayed, which strongly depend on the actuation behavior. Finally, a brief summary for the recent progress and the perspectives for the future development of the FSAs are made according to the discussions mentioned above.

Fabrication Methods

How to fabricate the FSAs is one important step in the FSA field, because the fabrication technology makes a critical difference on the actuation behavior of the FSAs to some extent. Up to now, researchers have spared no efforts to develop diverse technologies to realize the controlled fabrication of the FSAs. In this part, the typical fabrication methods will be discussed and compared.

Mold Shaping

Mold shaping is a relatively simple method to fabricate the FSAs. Typically, the raw reaction solution or polymer solution is injected into a tube-shaped mold, followed with a curing/solidifying process. After demolding, a solid fiber-shaped sample is obtained (Fig. 2I–III). For example, Lv et al. [25] injected azobenzene-containing linear liquid crystal polymer (LLCP) solution into a capillary glass tube. After the polymer was solidified, the mold of the capillary tube was etched by hydrofluoric acid to get a hollow fiber-shaped micro-actuator. Generally, some post-treatments are used to endow the fiber-shaped sample with the designed structures, so that the fiber owns the prescribed actuation

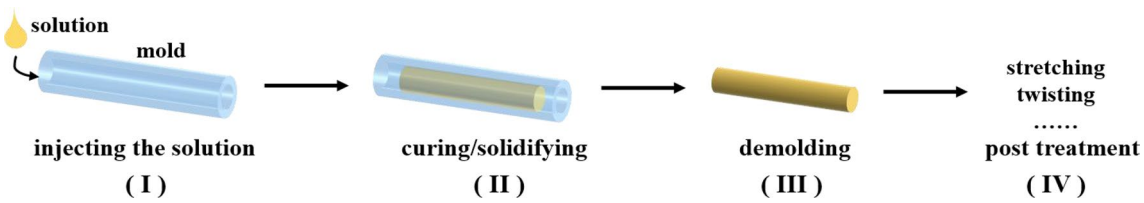

Fig. 2 Schematic illustration of the mold-shaping method to fabricate the FSAs

behavior (Fig. 1IV). Yu's group [26] reported a LCP-based FSA using the mold-shaping method; a mechanical stretching along the fiber axis was employed to induce the orientation of the LCP polymer. An and coworkers [27] reported a helical hydrogel-based FSA by the mold-shaping method combined with a subsequent twisting processing. The mechanical properties of the helical FSA such as tensile stress, strain and fracture energy are well related to the as-formed hierarchically arranged helical structures. The helical hydrogel-based FSA contracts and rotates in response to the water adsorption. This simple, direct and universal mold-shaping method still faces some obstacles that should be dealt with to get a well-defined FSA. For instance, during the curing/solidifying process in the mold shaping, the solvent evaporation sometimes will get into trouble, since the reaction/polymer solution becomes more and more sticky. As a result, it will generate some bubbles, leading to some flaws in the as-prepared fiber. Furthermore, the demolding should be careful, otherwise surface microcracking will occur. All the flaws on the fiber surface or in the fiber matrix will make an impact on the mechanical properties of the FSAs. Additionally, the resulting fiber structures (e.g., shape/size/length) are fully determined by the employed shaping molds. Thus, the variation of the fiber structures needs the change of the corresponding molds. The great challenge for the mold-shaping method is that the continuous production/fabrication of the FSAs is inaccessible.

Continuous Spinning

Spinning technology has been well developed for several decades and widely applied in the industry field to produce functional fibers in large quantities, such as polyester fibers [28], polyamide fibers [29], and aramid fibers [30]. The spinning process usually involves several important steps, e.g., as-spun fiber formation, drafting, and heat setting. In the stage of the as-spun fiber formation, the macromolecular chains are slightly oriented due to shear force when polymer solution or melt is extruded from a spinneret under pressure. During the drafting step, polymer chains of the as-spun fiber become highly oriented, which will induce the crystallization of polymer chains. Thereafter, heat setting is carried out to remove the as-formed internal stress, and the fiber with good dimensional stability and aggregation structure is finally generated. According to the routes to obtain the spinning fluid, spinning can be divided into melt spinning and solution spinning.

Melting Spinning

Melt spinning is suitable for polymers whose melting temperature is much lower than their decomposition temperature. During melt spinning, the extruded melt streams are gradually cooled down to solidify into continuous fibers. Melt spinning usually has the advantages such as a large production speed and no waste emission in comparison with solution spinning. Qi et al. [31] used the melt spinning in combination with ultraviolet (UV)-induced curing to fabricate ethylene–vinyl acetate (EVA) copolymer-based FSAs (Fig. 3). It is known that the drafting process can induce the orientation both for the stems in crystalline domains and for the segments in amorphous regions. This orientation can enhance the shrinkage of EVA-based FSAs when treated at a higher temperature than the glass-transition temperature. Meanwhile, the orientation ensures that the as-prepared fiber has a higher tensile strength than the counterpart. In their case, the subsequent UV irradiation-induced crosslinkage after melt spinning further solidifies the EVA-based FSAs.

Solution Spinning

Solution spinning, as the name implies, refers to the spinning preparation of fibers with polymer solution as spinning fluid. The solvent choice is of great importance for solution spinning. In addition, to attain the fiber with good structure and property, bubbles inside the spinning solution should be removed before spinning. According to the coagulation process, solution spinning can be further divided into dry spinning and wet spinning. For dry spinning, hot air or hot inert gas is introduced into the spinning channel to remove solvent from the spinning streams. For example, Roach and coworkers [32] prepared a long liquid crystal elastomer (LCE, a kind of cross-linked LCP with a low cross-link density)-based FSA using thermal convection to coagulate the extruded spinning solution. The precoagulated fiber was stretched between two mandrels to promote the mesogen orientation of the LCE. UV irradiation was subsequently conducted to fix the orientation. The diameter and actuation strain of the resulting LCE fiber can be tailored by the rotation speed of the mandrels, nozzle size and extrusion pressure. As for wet spinning, the spinning solution is extruded from a spinneret and immediately coagulated in a coagulant-containing bath. Using cold EtOH solution as a coagulant, Uh et al. [33] fabricated conductive polyaniline (PANI)-based microfiber through wet spinning. After stretching, the flexible PANI fiber can be processed into a straight, two-fly, knotted and spring form. Meanwhile, the fiber diameter can be tuned by the nozzle size. However, owing to the limitation of coagulation speed and the influence of flow resistance, the production speed using wet spinning is usually slower than that using dry spinning. Moreover, both wet spinning and dry spinning may cause environmental pollution since a large amount of solvent is used in the spinning process.

To summarize, the spinning methods mentioned above offer good choices for massive fabrication of FSAs with a

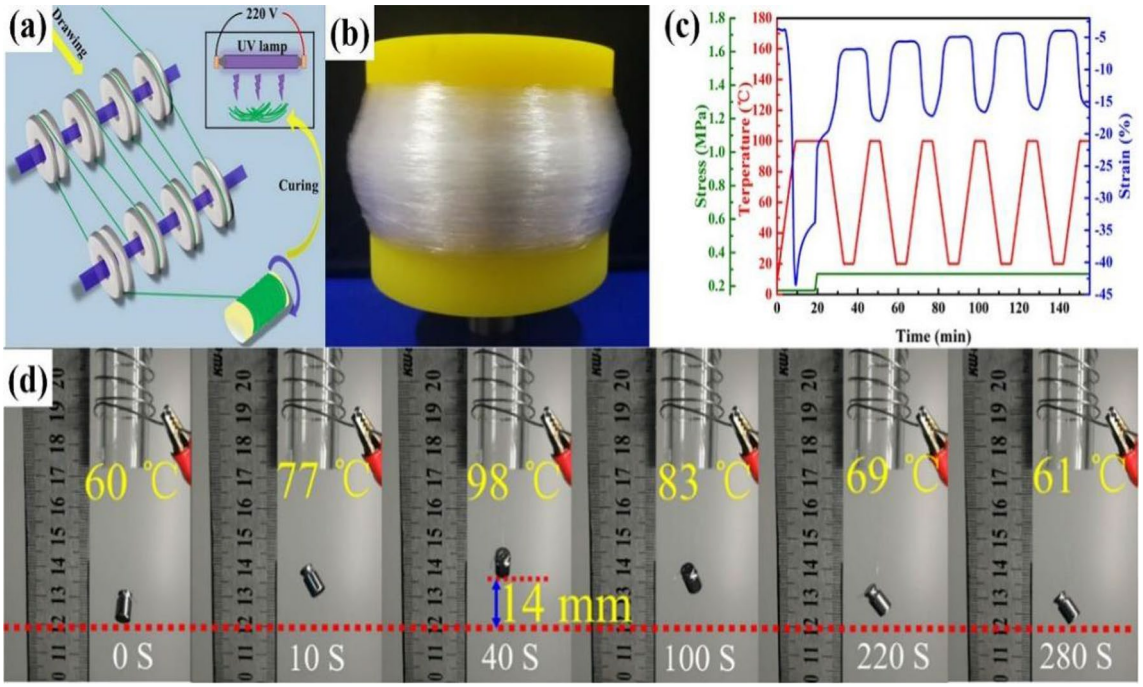

Fig. 3 **a** Schematic illustration of UV-assisted continuous spinning of EVA-based fibers; **b** Digital photograph of the as-prepared EVA fibers before UV curing; **c** Cyclic actuation behavior of the EVA-based FSA; **d** Digital photograph of the EVA-based FSA with a constant load under different temperatures; Reproduced with permission from ref [31], Copyright 2016, MDPI

controlled length and diameter. The spinning process can induce the orientation of the macromolecular chains of the FSAs, which plays a key role in the actuation behavior based on order change (which will be discussed in "Actuation Mechanism"). It should be noted that the morphology and mechanical property of the as-spun fibers are closely related to the spinning parameters, mainly including extrusion pressure, spinneret size, solidifying speed, drawing ratio, and the physical properties of the raw spinning materials. Furthermore, the viscosity of spinning fluid is much essential to keep the spinning process continuous and stable. To address this problem, investigators have put forward various strategies. For instance, nanoclay is added into the spinning solution to increase the viscosity and to maintain the stability of spinning process [32]. On the other hand, Terenthev et al. [34] provided a solvent-free spinning process to fabricate aligned LCE fiber. The constant temperature of spinning solution facilitates the stable flow of spinning solution. Meanwhile, an appropriate UV light is applied on the nozzle to initiate the crosslinking reaction. Upon exposure to UV light, the as-formed spinning gels can be easily drawn into a straight fiber and winded onto a rotating bobbin collector.

Fiber Twisting

As a routine operation step during the fiber preparation process, twisting is always used to clasp ready-made yarns together with the resulting enhanced properties and performances. Generally, during the twisting process, one end of the yarn is fixed while the other is rotated. As a result, the twisted fibers are in the form of spring-like structures (Fig. 4a, b). Because of these special structures, the twisted fibers exhibit intriguing actuation behaviors (e.g., contraction and twisting) responding to the variation of external stimuli (the mechanism will be discussed in "Actuation Mechanism"). In most cases, the twisted raw yarns own good affinity to water and other polar solvents, and thus the twisted fibers exhibit significant expansion perpendicular to the fiber axis. Lin et al. [35] reported a silk-based FSA with twisted structures, which could realize a rotation as fast as 6179.3° s^{-1} when exposed to water (Fig. 4c,d). Carbon nanomaterials with plenty of oxygen-containing function groups are widely used for the twisted fibers [20, 36, 37]. For instance, an FSA with twisted carbon nanotubes shows a nearly 50% contraction. In this case, the maximum specific work can arrive at 1180 J kg^{-1} stimulated by solvent absorption [36]. Meanwhile, the rapid improvement of the carbon-based fiber preparation technology enables the fabrication of high-performance FSAs composed of twisted carbon fibers [38, 39]. Furthermore, other functional materials can be integrated into the twisted FSAs with more desirable actuation behaviors [40–42]. For instance, nylon has the heating expansion ability, which is also considered to fabricate the twisted FSAs [40, 41]. Recently, Liu et al. [41] have twisted

nylon 6 fibers with carbon nanotube yarns (CNY) and then coated single-wall carbon nanotube (SWNT) on the surface of the twisted nylon 6 fibers. The as-prepared composite FSAs can be smartly driven by electro-heating. Jia et al. [42] proposed an interesting strategy to fabricate moisture-sensitive FSAs, i.e., folding the twisted fiber at the middle and attaching a load to make the two parts plied together spontaneously. Generally, the twisted fibers are mechanically unstable and tend to untwist. Thus the untwisting of the initially twisted fibers provides the twisting of plying that makes a torque-balanced torsional silk muscle. Furthermore, the authors coiled the twisted two-ply torsional silk on a mandrel and then fixed the structure by heating to obtain mandrel-coiled yarns of FSAs with reversible actuation (Fig. 4e). When the humidity increases, the FSAs whose individual fiber chirality matches the coil's chirality (homochiral) exhibit contraction while the FSAs with opposite chirality (heterochiral) elongate. Undoubtedly, twisting is a relatively simple method to prepare the twisted FSAs using the as-existing fibrous production. The actuation behaviors of the twisted FSAs can be controlled by various external stimuli based on different actuating principles, which will be discussed in the next part. It is pointed out that the accessible actuation behavior to these twisted FSAs is basically limited to the contraction and torsion, which will impose some restrictions on the practical applications.

Electrospinning

Electrospinning is a technique to prepare nanofibers constantly [43–48]. The main apparatuses involved in electrospinning are syringe, spinner, high voltage power supply, and collector (including tabulate, roller and drum according to the geometry shape) (Fig. 5a). The typical electrospinning process is as following. A high voltage electronic field is applied between the spinner and the collector. At the same time, the syringe is pushed forward at a certain rate. When the voltage increases to one critical value, the solution will jet out of the Taylor cone and towards the collector due to the applied field force. This is a complicated process, in which the jet flow will be separated and stretched helicoidally. Meanwhile, the polymer chains will be oriented and the diameter of fibers becomes smaller. Finally, the fibers are accumulated on the collector. The microstructures and arrangement of the spun nanofibers can be adjusted by the spinning needle and collector [43]. Generally, the electrospun nanofiber production is in the porous woven form. The pore size can be enlarged when the collection is performed in liquid in combination with the simultaneous sonication treatment (Fig. 5b) [44]. With the rapid development of the electrospinning technology, various kinds of electrospun nanofibers have been prepared, which have been widely applied in many fields [45–48].

Back in the early 2000s, polyurethane nanofibers with significant shape-memory property were prepared by electrospinning for the first time [49]. Afterwards, increasing attention has been paid to the development and application

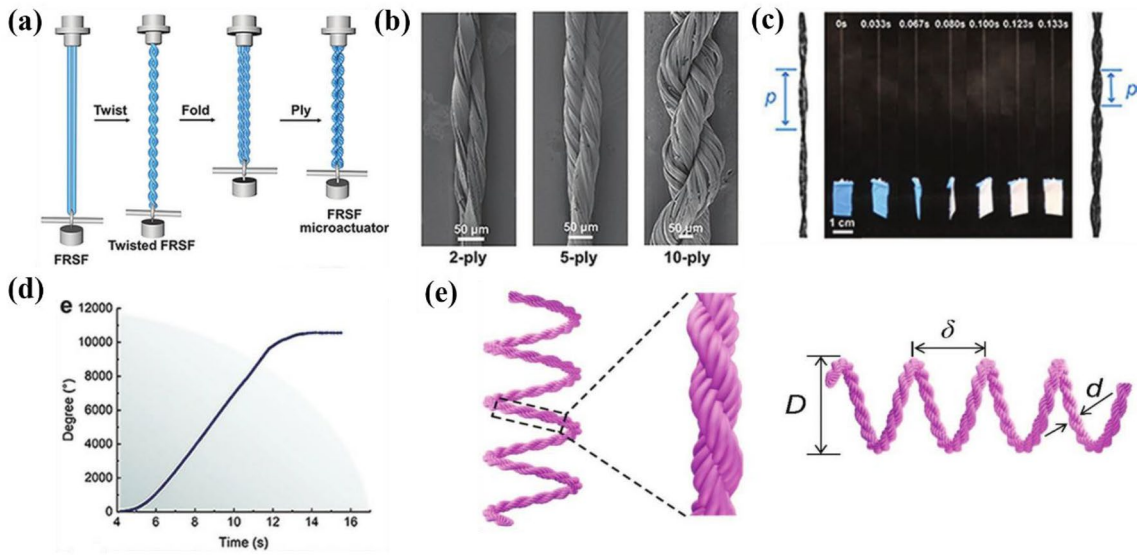

Fig. 4 **a** Schematic diagram of the fabrication process of the FSAs by twisting. **b** SEM images of the resulting FSAs with 2, 5, and 10 ply. **c** Digital photographs of working process of the twisted FSAs (p is the screw pitch). **d** Rotation angle as the function of driving time; Reproduced with permission from ref [35], Copyright 2020, WILEY–VCH. **e** Schematic illustration of a coiled FSA made from a two-ply torsional silk fiber; Reproduced with permission from ref [42], Copyright 2019, WILEY–VCH

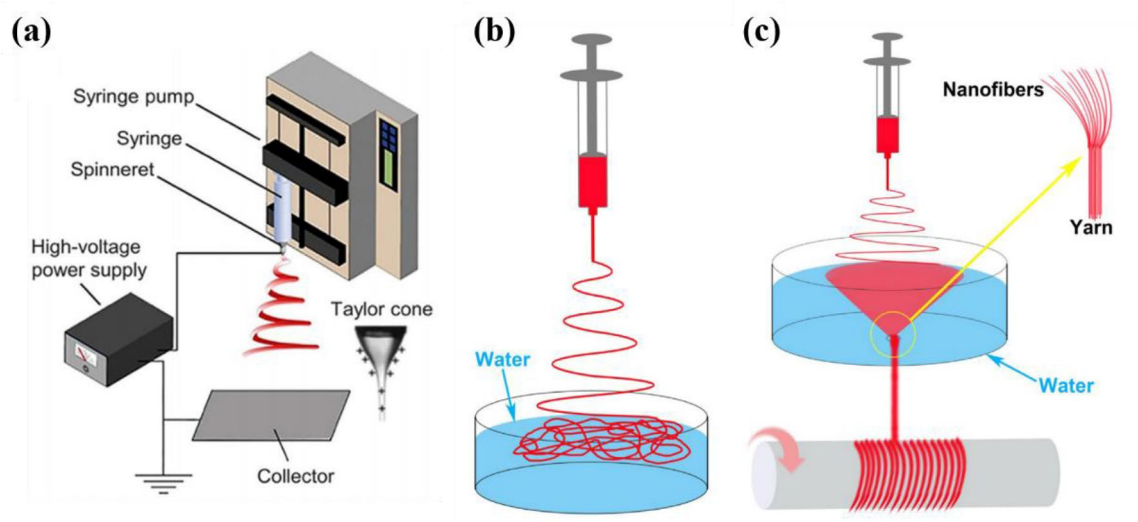

Fig. 5 Schematic diagram of the electrospinning technology: **a** Typical electrospinning device; Reproduced with permission from ref [48], Copyright 2017, American Chemical Society. **b** Electrospinning assisted with sonication treatment. **c** Water vortex-assisted electrospinning to fabricate aligned yarns; Reproduced with permission from ref [44], Copyright 2016, Elsevier

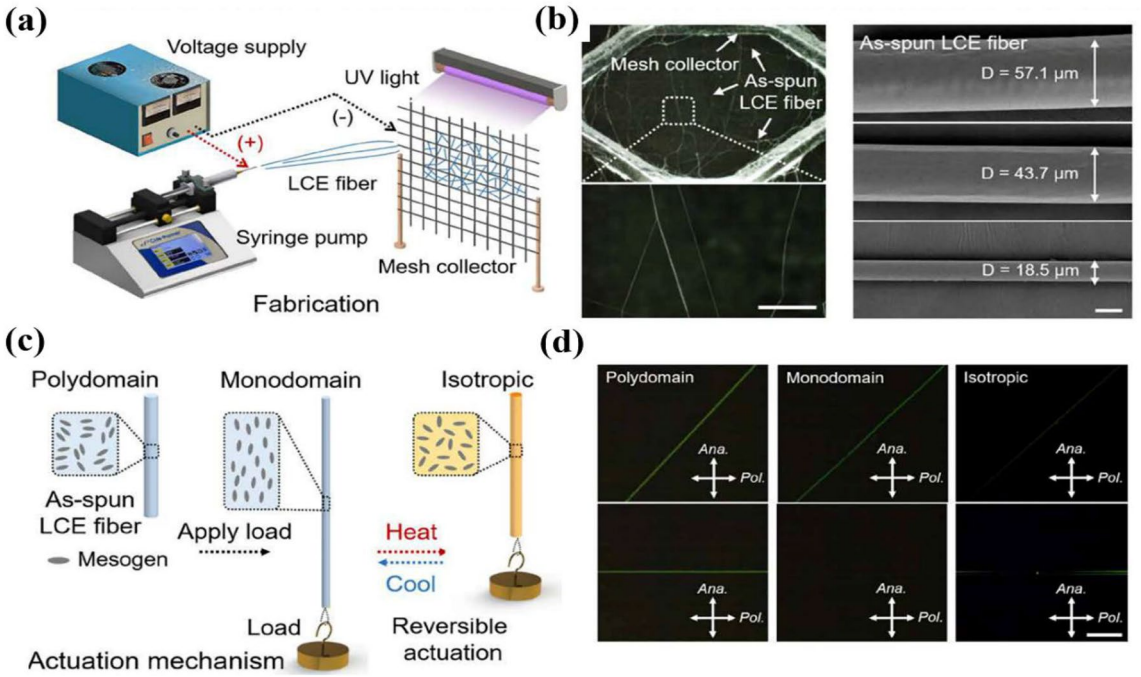

Fig. 6 **a** Schematic illustration of the electrospinning fabrication of LCE fibers. **b** Digital images (left) and scanning electron microscopy images (right) of the as-spun LCE microfibers with different diameters (Scale bars: 200 μm (left) and 20 μm (right)). **c**, **d** Actuation mechanism of the LCE-based FSA and corresponding polarized optical microscopy images of each orientation state (Scale bar: 200 μm); Reproduced with permission from ref [52], Copyright 2021, AAAS

of this electrospinning technique [50]. For example, polycaprolactone-based nanofibers with non-woven structure are fabricated by electrospinning [51]. Assisted with a water vortex, the as-spun nanofibers on the water surface can be pulled along the vortex and twisted as a continuous yarn (Fig. 5c) [44]. Recently, Cai's group [52] has developed a UV illumination-assisted curing process during electrospinning (Fig. 6). The as-fabricated bunches of LCE microfibers have the excellent reversible axial contraction behavior.

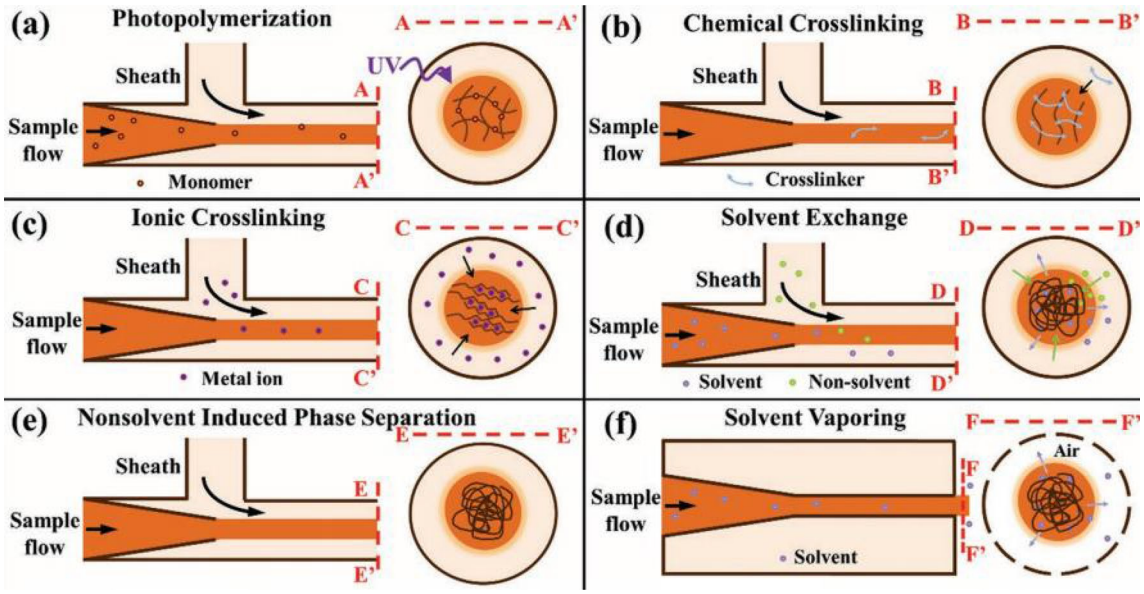

Fig. 7 Schematic illustration of different solidification methods for microfluid spinning. **a** Photopolymerization. **b** Chemical crosslinking. **c** Ionic crosslinking. **d** Solvent exchange. **e** Nonsolvent-induced phase separation. **f** Solvent vaporing; Reproduced with permission from ref [54], Copyright 2019, WILEY–VCH

Microfluid Spinning

In the early of 2000s, Jeong et al. [53] put forward the concept of microfluid spinning, which can be used to fabricate continuous gelatinous fibers. Nowadays, microfluid spinning has been developed into an emerging technology to fabricate various micro/nanoscaled fibers with diverse ordered structures, controllable compositions, and well-organized functions. As a typical microfluid spinning process, the polymer precursor fluid is introduced into a dependent input port. The fluid is shaped into various shapes by the used microchannels. Meanwhile, the fluid flow depends on the flow rate of the fluid and the structure of the microchannel. Afterwards, the shaped fluid flow is solidified into fibers with desired shapes and geometries. To precisely control the microstructures of the fiber production, the key is to control the laminar flow in the microchannel. The laminar flow is affected not only by fluid gravity and inertia, but also by fluid viscosity and surface tension. Interestingly, the multiphase laminar flows can be integrated precisely and each phase state in the channel can be regulated also. During this process, a rapid curing reaction is necessary to manipulate and restore the ideal fiber shape. So far, several solidification methods have been developed to enhance the curing process, which makes it possible to fabricate diverse continuous fibers via microfluid spinning (Fig. 7) [54].

Compared to the traditional continuous spinning methods, it is easier for microfluid spinning to fabricate continuous fibers with controllable sizes and geometries (e.g., flat, grooved, anisotropic, hollow, core–shell, Janus, heterogeneous, helical,

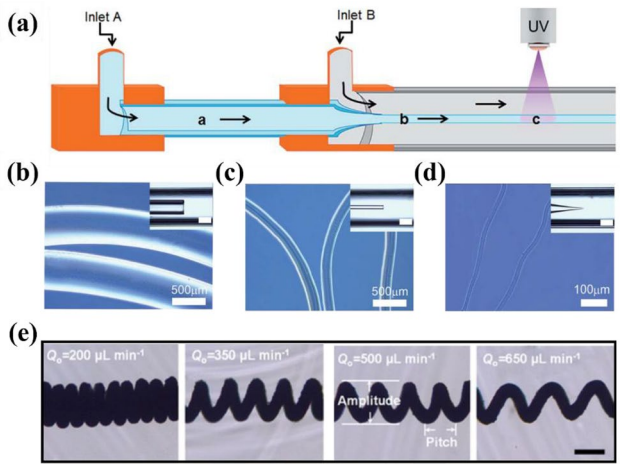

Fig. 8 **a** Schematic illustration of the fabrication of hydrogel-based FSAs by microfluid spinning. **b–d** Optical images of the obtained hydrogel-based FSAs fabricated with the inner capillaries (insert graphs, scale bars: 500 μm) of 590 μm, 150 μm and 10 μm, respectively; Reproduced with permission from ref [56], Copyright 2015, Royal Society of Chemistry. **e** Optical micrographs of the helical microfibers with different outer fluid flow rate (Q_0: outer fluid flow rate; an inner fluid flow rate: 200 μL/min); Scale bar: 300 μm; Reproduced with permission from ref [58], Copyright 2018, American Chemical Society

and knotted shapes) [55]. This is very helpful to tailor the actuation behavior of FSAs by means of the fiber microstructures. As shown in Fig. 8a–d, a hydrogel-based FSA with dual network structures is prepared by the microfluid spinning [56]. Similarly, Stannarius et al. [57] injected the raw materials

(including mesogen and crosslinker) into the laminar coflowing silicon oil to induce the parallel orientation of the mesogens relative to the flowing direction. During this procedure, UV irradiation initiated the cross-link reaction, leading to the desired LCE-based fibers with aligned structures. The components and microstructures can be modulated by the spinning parameter and materials, so that the actuation behaviors of the FSAs can be tailored conveniently. Tang et al. [58] selected a cylindrical capillary as an inner tube and a square one as an outer channel. Based on the liquid coiling effect, a coiled flow is formed stably when the viscosities and flow rates of the inner fluid match with those of the outer fluid. When the outer and inner fluids contact, Ca^{2+} in the outer fluid diffuses into the inner fluid to cross-link the alginate, so that the helical shape of the inner fluid is solidified in situ to generate helical microfiber. The helical microfiber with the length of 7 m can be fabricated continuously in 1 h, and the helical structure can be tailored by changing the fluid flow rate. Furthermore, these microfibers are further used as templates to fabricate FSAs with hollow structures. Currently, microfluid spinning offers a promising way to fabricate continuous fibers that can be applied for the FSAs. However, there are some challenges to be addressed in the further investigation. For instance, the candidate materials suitable for the microfluid spinning are still relatively limited.

3D Printing

In recent years, 3D printing technology has also been widely used to continuously fabricate fiber-shaped structures and the corresponding FSAs in bulk production. Molecular chains of the employed polymers could be oriented on account of the shear force when the materials are extruded from narrow spinning nozzles. As shown in Fig. 9a, the investigators from Harvard University fabricated diverse innervated LCE (iLCE)-based FSAs by this technology [59]. Notably, liquid metal (LM) was injected into the coaxial core at the same time during spinning. As a result, the reversible contraction behavior of these FSAs can be modulated by electric heating (Fig. 9b). Apart from LCP and some special polymers which have rigid units, this method is also feasible for other materials to fabricate fiber-shaped structures. For instance, electro-responsive hydrogel FSAs composed of poly(2-acrylamido-2-methylpropanesulfonic acid) (PAMPS) and poly acrylamide (PAAm) are prepared by the similar continuous approach named as self-lubricated spinning (SLS) (Fig. 9c–e) [60]. This approach realizes an effective production of FSAs in a large scale. There is no double that the 3D printing technology is flexible enough to fabricate various FSAs which are very suitable for complex working conditions.

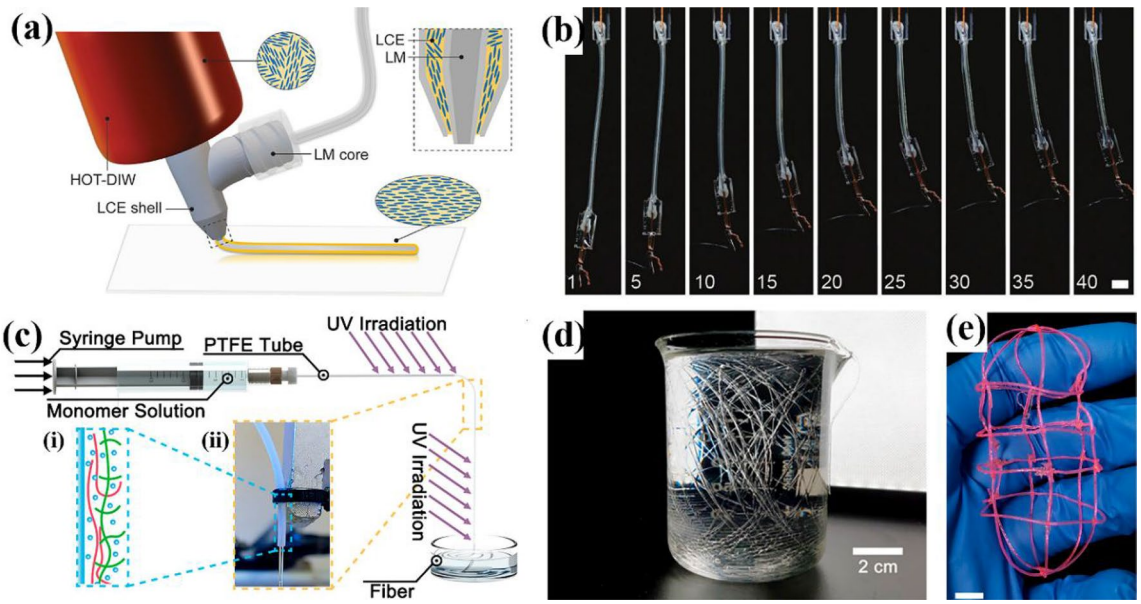

Fig. 9 **a** Schematic illustration of 3D printing process to fabricate iLCE fibers composed of a LM core surrounded by a LCE shell. **b** Digital photographs of the electric-driven actuation of iLCE FSA (Scale bar: 5 mm); Reproduced with permission from ref [59], Copyright 2021, WILEY–VCH. **c** Schematic illustration of the SLS fabrication process (thick blue line: tube wall, red line: PAMPS chains green line: PAAm network, blue dot: water molecule). **d** Digital photograph of the hydrogel FSAs in water. **e** Digital photograph of a hollow cage constructed by hydrogel FSAs (Scale bar: 1 cm); Reproduced with permission from ref [60], Copyright 2020, American Chemical Society

In conclusion, long FSAs with well-defined structures can be produced in large quantities by the continuous spinning technologies mentioned above. However, considering that all the parameters must be matched to each other, such as the properties of raw materials, process conditions and equipment status, these continuous spinning technologies are still relatively complicated.

Dipping-Pulling

When a tip is dipped into a liquid with a certain viscosity and then pulled up, a fibrous structure will be formed between the tip and the liquid surface. This simple dipping-pulling procedure has also been employed to fabricate the FSAs. For instance, Naciri and coworkers dipped the tip of a metallic tweezer into a nematic LCE prepolymer solution and pulled the tweezer as quickly as possible to yield a fiber-shaped structure [61]. After the polymerization was completed, the LCE fiber exhibited a reversible contraction of 30–35%.

It is pointed out that the pulling process promotes the mesogen orientation of the nematic LCE. According to the similar strategy, the LCE-based FSAs simultaneously with rotating structure and stretched structure have been fabricated recently (Fig. 10) [23]. In this case, a copper needle is used to dip and pull the prepolymer solution. During the pulling process, the needle is simultaneously rotated to induce the helical orientation of the mesogens. At the same time, in-situ exposure of the as-formed helical fibers to UV light is performed to accelerate the polymerization process. The resulting LCE-based FSAs can rotate to a certain angle and contract when subjected to UV illumination. Certainly, the fiber surface fabricated by this dipping-pulling method is not always smooth and the orientation of mesogens induced by pulling process is not well designed. As a result, the actuation behavior is not controlled precisely sometimes. Furthermore, the length of the as-prepared fibers via the dipping-pulling process is relatively limited. As for the employed raw materials, a certain viscosity for the

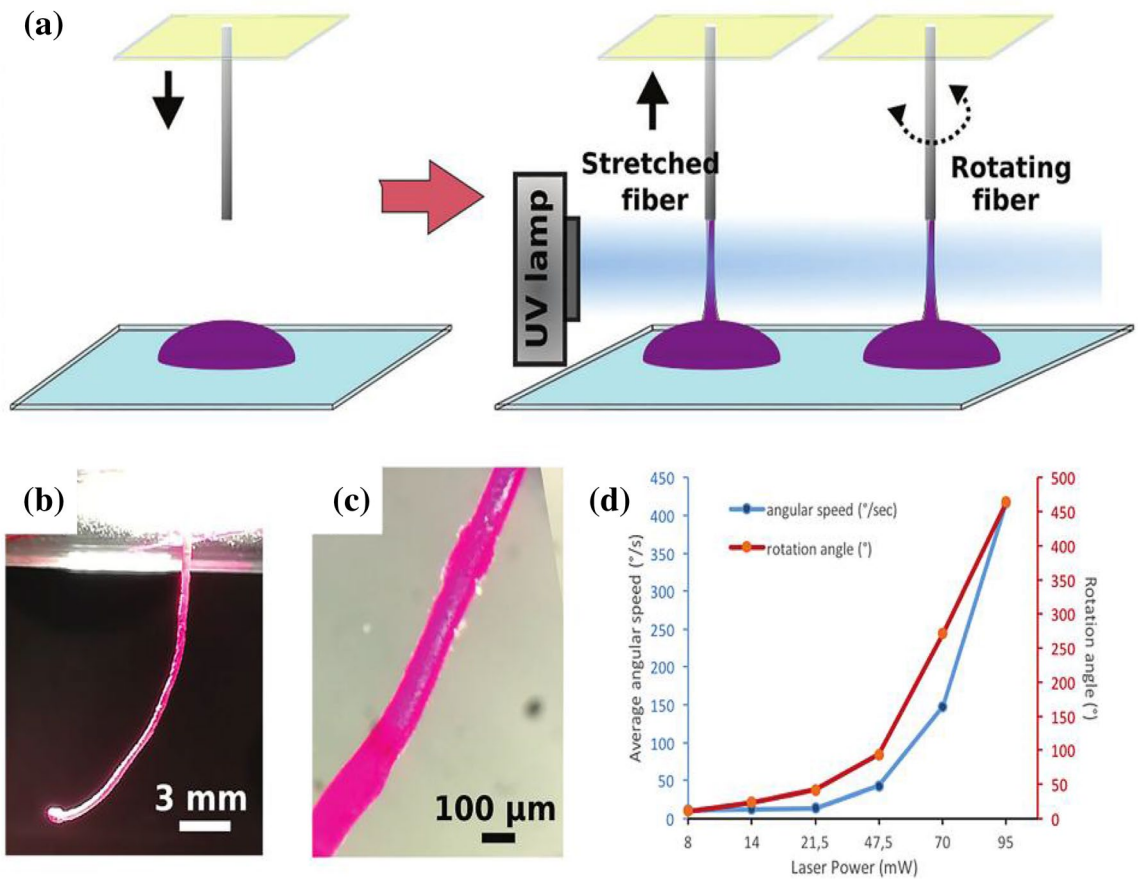

Fig. 10 **a** Schematic illustration of the process to fabricate a LCE-based fiber through dipping-pulling. **b**, **c** Optical image of the obtained fiber with a helical structure and stretched structure, respectively. **d** Average angular speed and rotation angle of the rotating fiber (1 mg) with a load (14 mg) under various laser power; Reproduced with permission from ref [23], Copyright 2017, Royal Society of Chemistry

Table 1 Comparison of different FSAs fabrication methods: typical material, structure, advantage, and disadvantage

Method	Material	Structure	Advantage	Disadvantage	Refs.
Mold shaping	LCP, hydrogel	Linear, helical, hollow	Simple process	Limited length	[25–27]
Continuous spinning					
Melting spinning	Polymer melt	Linear	Continuous, mass production	Complex equipment and parameter	[31]
Solution spinning	Polymer solution	Linear			[32–34]
Fiber twisting	Yarn	Twisted, helical			[20], [35–42]
Electro- spinning	LCP, SMP	Linear			[49–52]
Microfluid spinning	hydrogel, LCP	Linear, helical			[55–58]
3D printing	LCP, SMP	Linear	Continuous, mass production	Complex equipment and parameter	[59, 60]
Dipping-pulling	LCP	Linear, twisted	Simple process	Limited length, imperfect structure	[23], [61]

dipping-pulling solution is required to keep the stability of the fibrous structure during the pulling up.

Table 1 summaries the comparison of the above-mentioned technique for the fabrication of the FSAs. It is seen that each method has its internal advantages and disadvantages, the suitable raw materials and the resulting structures accessible to the FSAs. These methods also offer a wide platform to design and fabricate the FSAs with the controlled microstructures and the tunable actuation performances.

Actuation Mechanism

Various fiber structures fabricated by the above-mentioned technologies own different actuation behaviors under external stimuli. Actuation principles and actuation styles of the resulting FSAs are closely related to the fiber structures and material properties. Nowadays, more and more investigations have focused on how to design and control the actuation behavior of the FSAs via a relatively simple principle. In this section, the typical actuation mechanisms for the FSAs will be reviewed.

FSAs Actuation Based on Fluidic Actuation

Fluid-actuated FSAs are generally composed of a soft body and a fluid-tight hollow cavity. When the fluid pressure increases, the soft body will expand along the radial direction and shrink along the axial direction. By introducing specific structures or materials with various moduli to obtain asymmetric structures in the soft body, the resulting actuator can realize complex motions [62]. This can be ascribed to the different deformation abilities of different parts in the soft body under the pressure. Paek et al. [3] fabricated an asymmetric microtube with an end-facet sealed by poly(dimethylsiloxane) (PDMS) elastomer. Compared to the thicker wall, the thinner one owns a lower modulus and exhibits a more obvious expansion, leading to the bending towards the thicker wall owing to a pneumatic actuation. By means of adding a hump-like structure at a suitable position, a larger bending as well as spiraling can be realized (Fig. 11a, b).

In the middle of last century, Mckiben designed a novel artificial muscle (named as Mckibben muscle) with an inner elastic bladder surrounded by a woven or braided sheath. It is a typical pneumatic-driven FSA. Notably, the surrounding fibers are not aligned in the axial direction relative to the inner bladder, but at an angle (α) relative to the axis [63] (Fig. 11c). When the bladder is filled with fluid, the sheath will restrict the radial expansion of the bladder. If $\alpha < 55°44'$, the bladder shows a contraction behavior (named as contractile Mckibben muscle). If $\alpha > 55°44'$, the bladder shows an elongation behavior (named as elongated Mckibben muscle) [64]. Based on this archetype, Suzumori et al. [4] proposed muscle textiles consisting of multiple soft thin Mckibben muscles to improve power output and flexibility. Furthermore, they designed an active textile braided in three strands, which can provide a larger contraction ratio than a single Mckibben muscle [65]. Compared to the conventional fluid-actuated FSAs, Mckibben muscle can generate more acceleration and move to the target position smoothly, which is useful for practical applications. However, the attached bulky pneumatic compressor is unsuitable for the human-friendly application. To deal with this problem, Cacucciolo et al. [66] integrated a stretchable pump (electrohydrodynamics, EHD) with a thin Mckibben muscle. Compared to the traditional Mckibben muscle system, this device is lighter, slender, and easier to be bent or twisted largely (Fig. 11d). The design strategy and working mechanism of EHD are presented in ref [67]. On account of the friction between the bladder and the textile sheath, the Mckibben muscle generally can not recover to the initial shape after an actuation is completed. The bladder of Mckibben muscles is usually made of tough rubber-based materials, and thus the pressure applied to drive the device is high

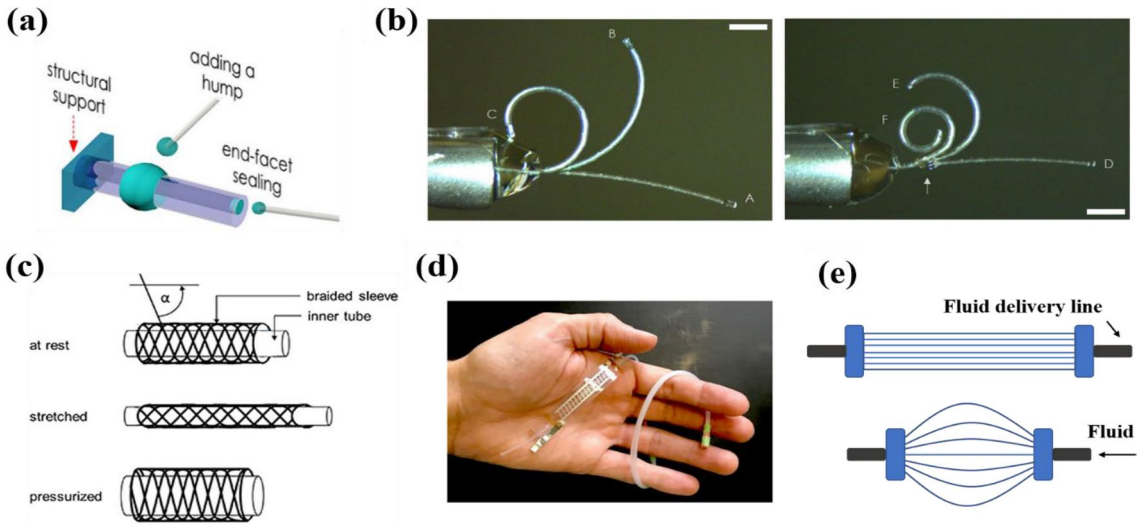

Fig. 11 **a** Schematic diagram of the microtube FSAs with a hump. **b** Bending deformation of the microtube FSA without a hump (left) and with a hump (right) (Scale bar: 1 mm); Reproduced with permission from ref [3], Copyright 2015, Nature. **c** Schematic illustration of the Mckibben muscle; Reproduced with permission from ref [63], Copyright 2022, IOP Publishing Ltd. **d** Digital graph of the thin Mckibben muscle with stretched pump; Reproduced with permission from ref [66], Copyright 2022, Frontiers. **e** Schematic illustration of the pleated Mckibben muscle

(typically about 90 kPa) with the resulting deformation ratio of about 20–30% [68]. To solve these problems, a new generation of Mckibben muscle with pleated structure is developed. Here the membrane is folded along its central axis and connected to the end of fluid delivery line. When a fluid pressure is applied, the muscle will shorten and swell into a lantern-like shape (Fig. 11e). Since the used membrane with high tensile strength is highly flexible, this kind of pleated FSA can realize a larger deformation and generate a force of 3500 N under a relatively low power input [63].

Apart from the actuation by fluid pressure change, Li et al. [69] reported the actuation of hollow fibers by hot fluid. This FSA that is based on low-density polyethylene hollow fibers (PEHFs) exhibits the expansion in the radial direction and the contraction in the axial direction. This shape variation is related to the highly oriented semicrystalline form of PE, which is a kind of taut tie molecular morphology formed during the fabrication process. The PEHFs are in the twisted shape at first. When hot liquid is injected into these FSAs, the twisted fibers exhibit a torsional rotation on account of the volume expansion and the activation of segment orientation. When the twisted fibers are further shaped into coil structures, the coil geometry induces the convertion of the rotation actuation into a spiral actuation.

FSA Actuation Based on Volume Change

Some materials with special microstructures can perform a volume change when external conditions vary. This kind of volume change has been well utilized to drive the actuation of some FSAs. It is known that hydrogels are physically or chemically bonded three-dimensional polymer networks with large amount of water entrapped in intermolecular space. In the last century, Tanaka et al. [70–72] have reported that the environment fluctuation can be utilized to drive a reversible volume change of hydrogels (more than 10 times in volume). In their case, the stimulus-responsive hydrogels are composed of hydrophobic groups and polar groups in the molecular chains. When the surrounding conditions (e.g., the temperature [73], pH [74] and solvent concentration) vary, the swelling capacity of hydrogels to some matter combining with the crosslinking state will change. Hence, a significant mass exchange between the hydrogel and environments occurs, and the hydrogel will expand or shrink in macroscale. The hydrogel will not be dissolved because of the crosslinking structure [75]. Hereinto, thermo-sensitive hydrogel is one of the most common hydrogels with the stimulus-responsive ability. In most cases, the temperature variation will affect the hydrophilicity/hydrophobicity of hydrogel networks. For the hydrogels with the lower critical solution temperature (LCST), a reversible swelling/shrinking can be switched by the temperature (i.e., shrinking (or low swelling) at a high temperature and high swelling at a low temperature) (Fig. 12a) [76, 77]. Based on this actuation principle, many hydrogel-involved FSAs have been fabricated. For instance, Jalani et al. [78] fabricated bimorph hydrogel-based FSA with electrospinning-induced helical structure. One side of this FSA that is made of thermo-sensitive hydrogel with LCST is sensitive to the temperature, while the other side is inert to the temperature. When the temperature is above the

LCST, the FSA transforms from the helical structure into a linear structure due to the shrinkage of the sensitive side. For pH-sensitive hydrogels, there exists physical interaction between polymer chains. If the environmental pH changes, the interaction strength will decrease (or increase), and the crosslinking density will change accordingly (Fig. 12b) [74]. In most cases, the volume change of hydrogels is isotropic. Furthermore, the mechanical strength of this material is always not high enough to satisfy the practical scenarios, especially for the hydrogel-based FSAs as artificial muscles or other joint elements. To meet this end, a hydrogel-based FSA coated with carbon nanotubes (CNTs) has been reported [79]. The CNTs sheath not only improves the water tolerance, but also enhances the tensile strength of the final hydrogel-based FSA.

In the electric field, positive and negative ions will directionally move toward to the corresponding opposite electrode. Compared to the cathode-contacted side, the anode-contacted side of hydrogel-based actuators always expands more visibly owing to larger negative ions accumulated. Hence, the electrosensitive hydrogel-based actuator exhibits a bending deformation towards the cathode side [80, 81]. Duan and coworkers [60] immersed a hydrogel-based FSA into an electrolyte solution. When the electrolyte solution was electrified, the immersed FSA bent directionally (Fig. 12c, d). A bimorph hydrogel-based FSA composed of graphene and polypyrrole displays an obvious bending behavior in the electrified electrolyte solution based on the similar principle [82]. Here, the mass exchange for the FSAs always takes place in the solution environment, making it difficult to achieve the rapid actuation, especially for hydrogel-based ones. To address this problem, Chen et al. [83] put forward a new bilayer hydrogel-based FSA. The two hydrogels have different critical solution temperatures. When the temperature changes, water molecules will transport between the two layers so that the bilayer hydrogel-based actuator can perform the actuation without a liquid environment. The bilayer hydrogel-based FSA shows the application potential especially in the organism with rich and variable liquid conditions.

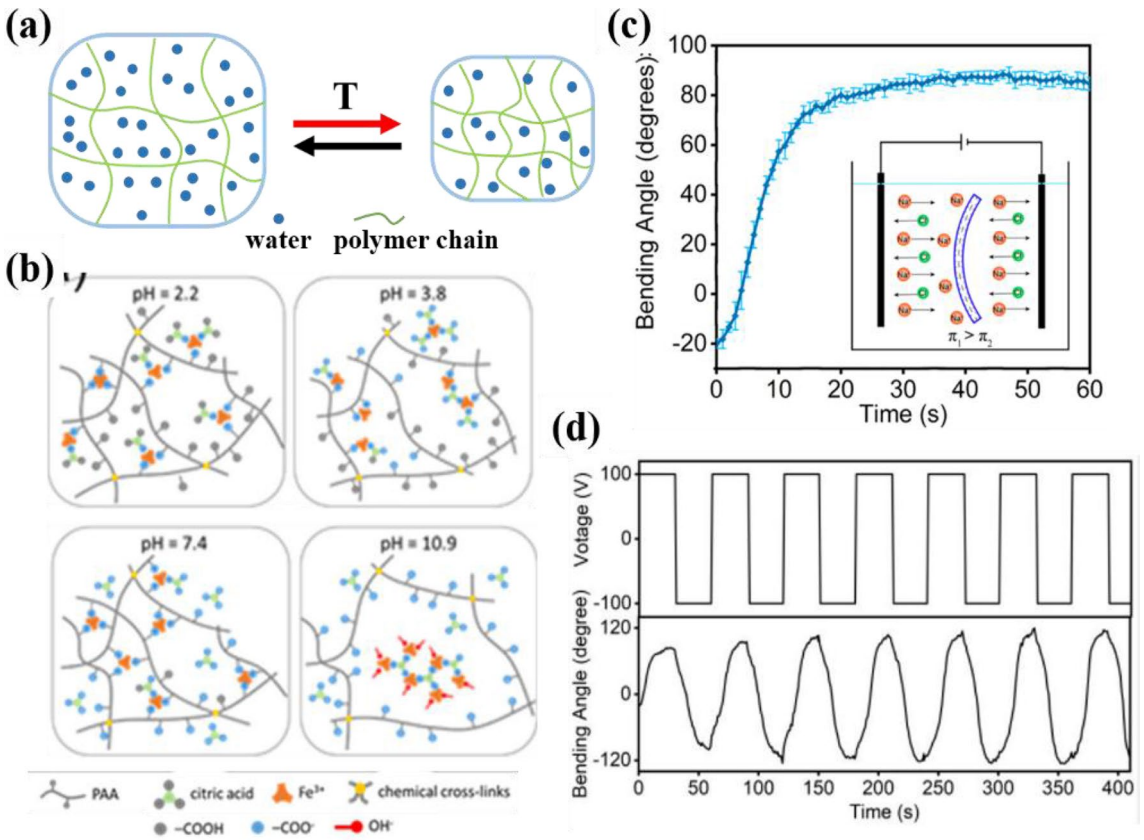

Fig. 12 **a** Schematic illustration of the thermo-sensitive hydrogel. **b** Schematic illustration of the pH-sensitive hydrogel; Reproduced with permission from ref [74], Copyright 2019, American Chemical Society. **c** Electro-driven actuation of the hydrogel-based FSA (insert: mechanism illustration). **d** Cycle performance of the electro-driven actuation of the hydrogel-based FSA (field strength: 0.5 V mm^{-1}); Reproduced with permission from ref [60], Copyright 2020, American Chemical Society

FSA Actuation Based on Order Change

When the molecular chains go from an oriented state to a random state under external stimuli, the material will show a shape change at macro scale, e.g., shrinking in the original orientation direction and expanding in the orientation-vertical direction. This order change-induced shape deformation is one important principle to design soft actuators including the FSAs.

Liquid crystal (LC) is one kind of unique materials both with the fluidity of liquid and the ordered molecular array of crystal. The orientation state can be varied reversibly by the environment change. Introduction of LC into polymer (i.e., the formation of liquid crystal polymer (LCP)) was first proposed by Vorlander's team in the last century [84]. Afterwards, Jackson et al. [85] prepared a series of LCPs in their laboratory. Due to the macromolecular structure, LCPs possess higher mechanical strength and thermal stability than the small molecular counterparts. Furthermore, the mesogen units in the LCPs endow the LCP-based materials with ordered microstructure and stimulus-responsive ability. As mentioned in "Fabrication Methods", some treatments, such as mechanical stretching and shearing, can induce the molecular chains of LCPs into an ordered state. Under some certain stimuli, the variation of mesogen orientation drives the movement of the segments for LCPs. This provides broad prospects to fabricate functional deformable materials based on LCPs. As one widely used photosensitive molecule, azobenzene owns intriguing *cis–trans* photoisomerization and is frequently incorporated to obtain photosensitive LCPs [86, 87]. Under UV illumination, the order state of molecular chains of the azo-containing LCPs will change significantly because of the *cis–trans* photoisomerization of azobenzene (Fig. 13a,b,d). Based on this photochemical reaction of azobenzene moieties, Pang et al. reported an interesting light-driven FSA composed of azobenzene-containing linear LCP [26], which owns a large contraction up to 81% upon the 470 nm light illumination (Fig. 13e). On the other hand, cross-linked LCPs with a low cross-link density not only have the anisotropy and stimulus-response ability of non-crosslinked LCPs, but also own the elasticity of polymer networks [88, 89], which broadens the application of LCPs for the FSAs. Recently, the FSAs composed of azobenzene-containing cross-linked LCP have been reported, which exhibit a quick and large bending deformation away from the light source [90]. It is concluded that the position of azobenzene units in the molecular chains takes a critical role in the light-driven bending motion. However, UV is harmful to living organisms, which poses an obstacle to the practical applications of the azobenzene-containing smart materials in the related fields.

Additionally, the temperature change can be regarded as one factor for the phase transition of LCPs. For instance, when the temperature increases above the phase transition

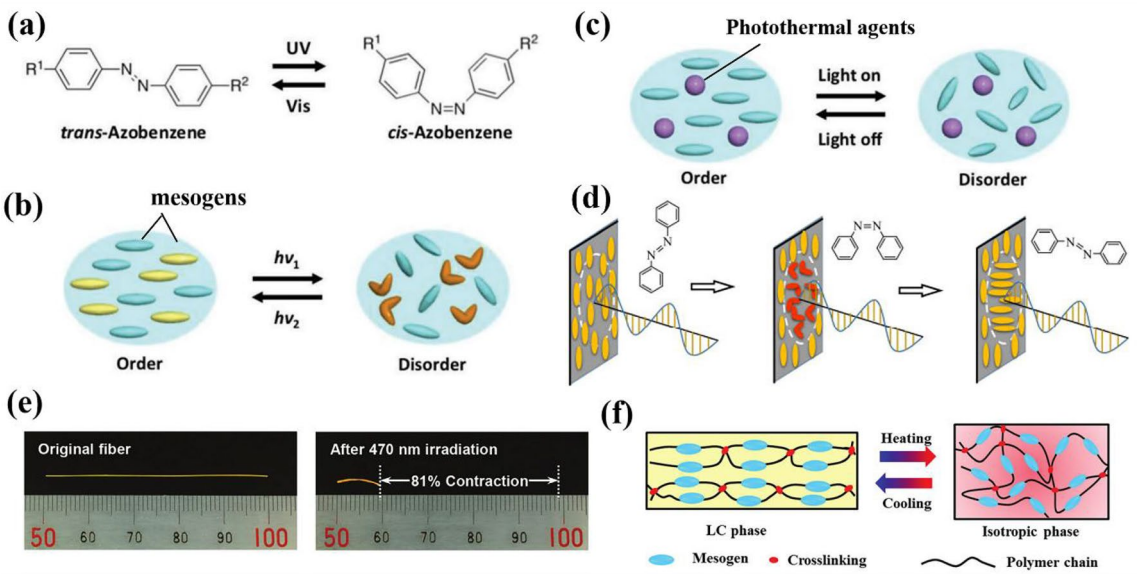

Fig. 13 **a** Schematic illustration of reversible *trans–cis* photoisomerization. **b** Photo-induced and **c** photothermal-induced order–disorder phase transition of azobenzene-containing LCPs; Reproduced with permission from ref [86], Copyright 2019, WILEY–VCH. **d** Photo-induced reorientation of azobenzene-containing LCPs with linearly unpolarized light; Reproduced with permission from ref [87], Copyright 2017, Science Press. **e** Digital photographs showing light-driven contraction of the LCP-based fiber upon irradiation (470 nm, 100 mW cm^{-2}); Reproduced with permission from ref [26], Copyright 2020, WILEY–VCH. **f** Schematic illustration of the reversible macroscopic shape change of cross-linked LCPs caused by thermal-induced aligned LC-isotropic phase transition; Reproduced with permission from ref [94], Copyright 2018, Royal Society of Chemistry

temperature, the oriented mesogens become randomly aligned. When the temperature goes down, the mesogen orientation recovers spontaneously and the shape of the material goes back to the initial state (Fig. 13c,f) [91–94]. Hereinto, photothermal reagents are integrated into the LCP matrix to realize the optical control of the actuators with the help of photothermal conversion [91, 92]. It has been reported that under the illumination of an impulse near infrared (NIR) light, electrospun LCE microfibers coated with polydopamine (PDA) exhibit a fast reversible contraction behavior [52]. The largest actuation strain is nearly 60%, which decreases with the increase of the illumination frequency. With a certain load, the PDA-coated LCE microfibers can contract reversibly more than 10^5 cycles without an obvious fatigue. Compared with other stimuli, light illumination has unique advantages such as remote, spatiotemporal and non-contact control. Since the illumination strength decreases along the fiber diameter direction, a gradient change in the fiber microstructure will occur under the light illumination. Therefore, some light-driven soft actuators show a movement toward or away from the light source. Yu et al. [93] investigated the NIR-driven phototropic bending behavior of one LCE-based FSA. It is indicated that the fiber size (length and diameter) and illumination conditions (power intensity, light source direction and light spot diameter) influence the bending deformation. Despite the significant advantages of the LCP-based FSAs, the trigger temperature of some thermo-sensitive FSAs is relatively higher, which puts an inevitable obstacle to the practical application especially in biological scenarios.

As another kind of smart soft materials, shape-memory polymers (SMPs) have also been widely used in soft actuator field [95, 96]. Typically, SPMs have the ability to change the shape through the switch between a permanent phase and a reversible temporary phase. The permanent phase consists of physical or chemical cross-linked network, determining the permanent material shape [97]. The reversible phase is composed of the segments without crosslinking, determining the temporary shape [98]. Under certain external stimuli, the segments of reversible phase are activated, and the SMPs will be shaped into a temporary shape. When the stimuli are removed, the activation for the mobility of segments will be frozen to keep the temporary shape. The fixed temporary shape is a thermodynamically unstable state with a relatively lower entropy. When the material is exposed to the stimuli again, the frozen mobility of segments will be activated. As a result, the external stimuli drive the switch between a permanent shape and a temporary shape for the SMPs. Nowadays, SMPs with multiple-shape memory ability have aroused intense attention. These SMPs are always available through a multi-step processing. Qi et al. [31, 99] prepared ethylene–vinyl acetate copolymer (EVA) fibers through UV illumination-assisted melting spinning (Fig. 14). The initially spun fibers were stretched twice under different temperatures and tensile forces to generate two temporary shapes. During this shape change process, two different orientations and crystalline phase transitions and conformational relaxations are involved. As a result, the as-prepared EVA fibers have outstanding triple-shape memory effect (triple-SME). Similarly, by regulating the ordered crystalline structure, a class

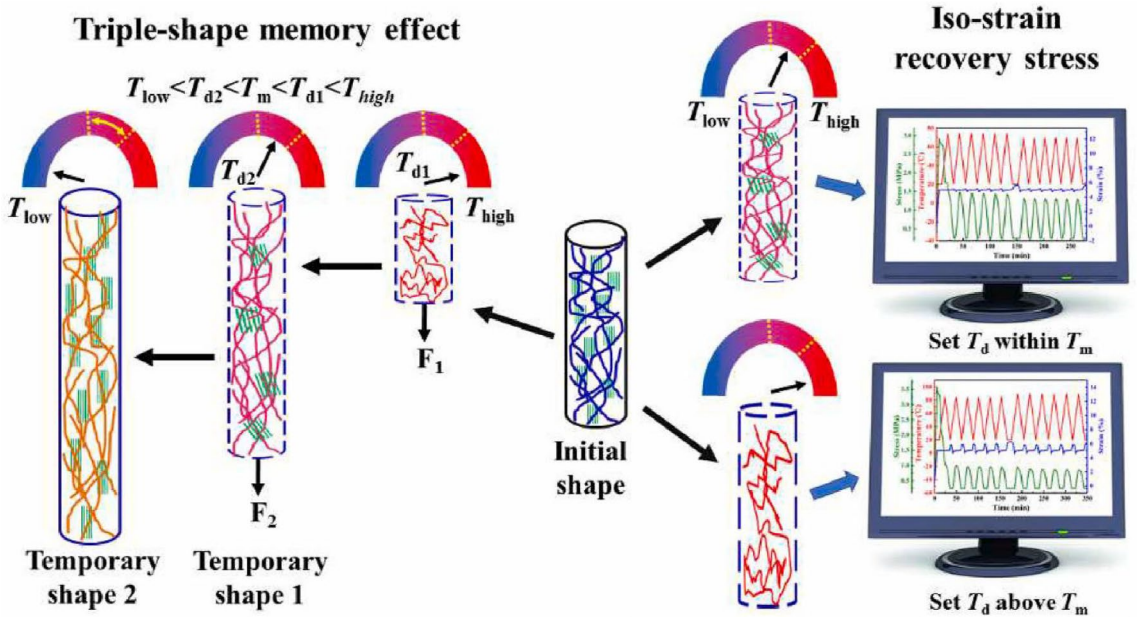

Fig. 14 Schematic illustration of the mechanism of triple-SME and recovery stress of EVA fibers; Reproduced with permission from ref [99], Copyright 2021, Elsevier

of FSA has been reported [100], which shows a controlled actuation behavior and highly desired mechanical properties. In this work, the linear triblock copolymer, poly(styrene)-b-poly(ethylene oxide)-b-poly(styrene), is introduced into an oriented fiber. The resulting fiber has a significant reversible contracting actuation that is stimulated by the changes in moisture and temperature thanks to the alternate crystalline nanostructure and amorphous region. Apart from being triggered by temperature fluctuation to induce the melting or crystallization for the crystalline structure, introduction of conductive filler into the SMPs matrix can realize the electro-driven actuation of SMPs via the joule heating. Meanwhile, it has been proved that water can cause the change in the interaction conditions for intermolecular/intramolecular hydrogen bonds [101]. Cera et al. [102] reported a keratin-based system with hierarchical structure. The shear force in the spinning process induces the self-organization of keratin protofibrils into a nematic phase. Depending on the metastable reconfiguration of the keratin secondary structure, which means the transition from α-helix to β-sheet, the resulting FSA exhibits water-stimulated shape-memory property. With the improvement of modern processing technology such as spinning and nano-imprinting [103], SMPs show certain internal advantages over other soft smart materials when used for the FSAs. However, there are still some obstacles to be addressed for the further practical application. For instance, reusable smart materials for SMPs are highly required, which could be reconstructed according to the application conditions [104].

Shape memory alloys (SMA) are one kind of alloys with shape-memory property, which have a large number of applications in the fields of industry and medicine. One of the most widely used SMA is nickel–titanium (NiTi) alloy, which was first discovered in 1960s. The shape change process of SMA can be described as the transition between two distinctive crystalline configurations, martensite and austenite. Martensite is stable below the phase transition temperature, while austenite is stable above this transition temperature. When the temperature goes up, the crystallic configuration will transfer from martensite to austenite. As shown in Fig. 15, by applying a certain load, the initial SMA fiber is stretched to a certain length (state A, martensite configuration). When heated above the transition temperature, the SMA fiber will shorten (state B, austenite configuration). If the temperature decreases afterward, the SMA fiber will recover to the initial length to some extent (state C, martensite configuration). Buckner et al. [105] shaped rod-like SMA fibers into a ribbon-like shape and then integrated them into a smart textile. During the shape change process, the highly flexible textile generates off-center force and results in a twist deformation for the SMA fibers.

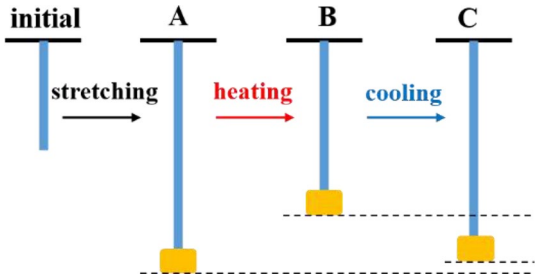

Fig. 15 Schematic illustration of the actuation mechanism of a SMA fiber

Dielectric elastomers (DEs) can be used as electromechanical transducers, because DEs can convert or transduce electrical energy to or from mechanical energy. DEs are always used in the form of a sandwich-like structure (e.g., a dielectric polymer material inserted between two electrodes). When a voltage is applied, charges will be accumulated on the two electrodes. The same charges repel each other while the opposite ones attract. According to the Maxwell' equations, the resulting stress will squeeze the polymer material, leading to a contraction along the electric field direction and an elongation perpendicular to this direction. After switching off the voltage, the system will recover to the original state [106–108]. When DEs are used as the FSAs, the general strategy is to prepare a coaxial core/shell structure where a soft dielectric polymer is sandwiched between two soft conductive electrodes (Fig. 16a). To obtain the excellent actuation performance, the electrodes should be bonded with dielectric as tightly as possible, and their stiffness should be as low as possible [109]. Based on this core/shell structure, Kofod et al. [110] prepared a DE-based FSA, which could show an elongation strain of approximately 7% under the stimulation of 7 kV. For tube-like DE-based FSAs, the applied prestrain, including uniaxial strain and uniform strain, affects the actuation behavior. Namely the axial actuation strain decreases while the radial actuation strain increases with the increase of prestrain [111]. Shimizu et al. [112] used sodium chloride solution as the aqueous electrode to drive a DE-based FSA under water. Generally, the DE-based FSAs offer distinct benefits over other FSAs in the electric control mode because they may be easily linked with the existing well-developed electrical systems to provide more accurate actuation behavior. However, there are still certain issues for the DE-based FSAs. For example, the available actuation strain and cycle life for the DE-based FSAs are not better than those for other FSAs; the driving voltage is significantly greater than the safe voltage. With the development of novel materials and fabrication technologies, those problems are now being solved gradually. Recently, Chortos et al. [113] have fabricated a DE-based FSA by a multicore-shell 3D printing strategy, in which the

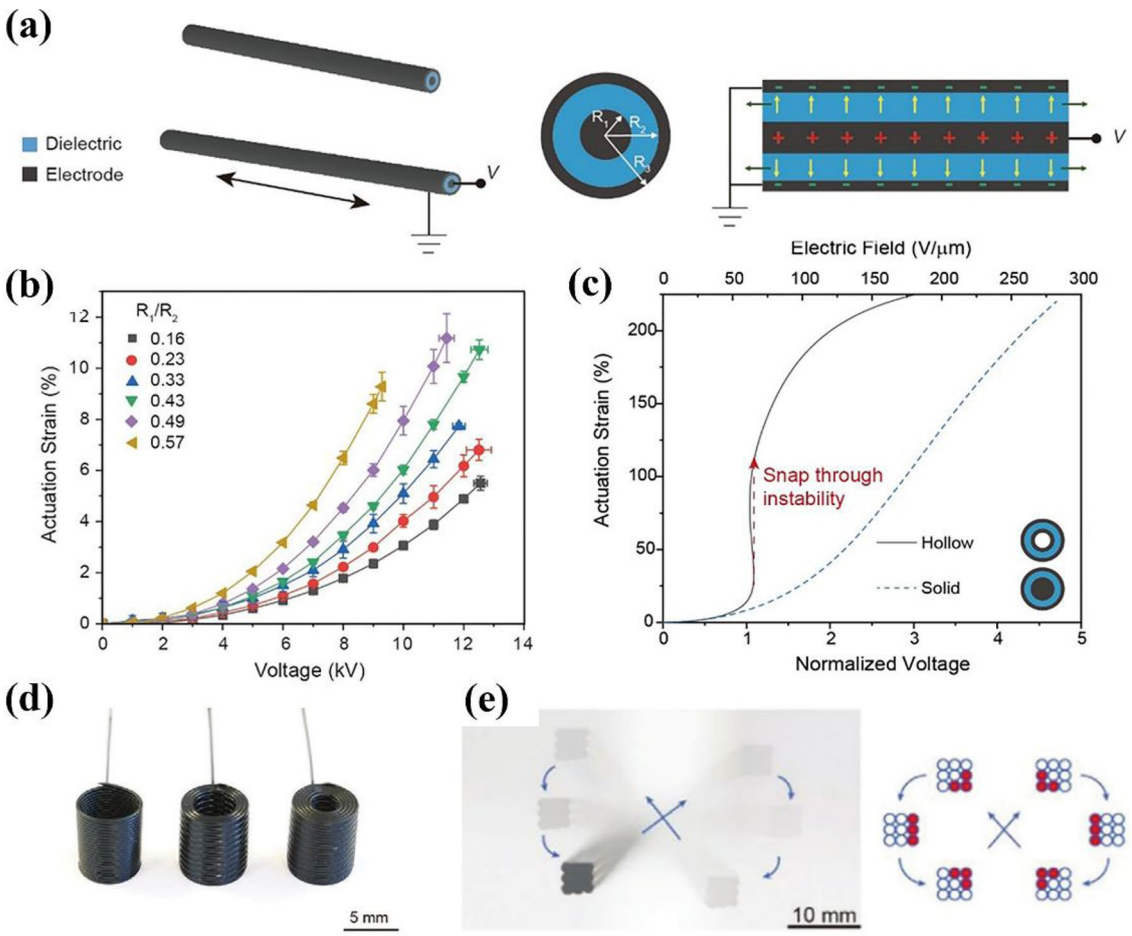

Fig. 16 **a** Schematic illustration of the actuation mechanism of the DE-based FSAs. **b** Actuation strain as a function of applied voltage for the DE-based FSAs with various R_1/R_2. **c** Actuation strain as a function of normalized voltage for the DE-based FSA with hollow-core structure and solid-core structure, respectively. **d** Digital photographs of the DE-based fibers with 1, 3 and 5 turns. **e** Swing track of the end of DE-based fiber bundle (left) and the schematic illustration of corresponding addressable sequence; Reproduced with permission from ref [113], Copyright 2021, WILEY–VCH

thickness of each layer and the fiber length could be flexibly controlled. It is found that the voltage required to realize the actuation strain decreases with the increase of R_1/R_2 (R_1: core electrode radius, R_2: dielectric sheath radius) (Fig. 16b). Furthermore, the greatest actuation strain can be up to 10%. According to the experimental and theoretical results, the DE-based FSA with solid-core structure is more stable than the hollow-core one (Fig. 16c), since the existence of the linear relationship between the applied voltage and actuation strain ensures the DE-based FSAs from electrical failure. Based on the fiber-shaped structures, diverse DE-based FSAs with vertical coils and fiber bundles have also been fabricated (Fig. 16d, e), which exhibit flexible actuation style and outstanding lifetime (exceeding 2.6 million cycles).

Tendril-like structures are common in nature. Inspired by these distinctive structures, lots of smart devices including sensors and actuators have been designed [114]. According to the Gibbs free energy, stretched amorphous polymer chains with partial crystalline structure tend to spontaneous relaxation (entropy increase) when the temperature increases. Hence, the stress in the stretched chains drives the material to contract at macroscale along the axial direction, which can be well used to design a new kind of FSAs. Haines et al. [40] fabricated tendril-shaped FSAs by overtwisting nylon fibers and polyethylene fibers, respectively (Fig. 17a). The decrease in partial crystallization in the stretched polymer chains causes the two kinds of fibers a small shrinkage (about 2%). However, the contraction ratio can increase dramatically to 49% if single fiber is twisted and the cycle life can arrive at more than 1 million when the test temperature is cycled between 25 and 150 °C. It is revealed experimentally and theoretically that the torsional actuation of the tendril-like structures plays the critical role in the reversible large-stroke actuation. A deep analysis about the tendril-shaped FSAs has been reported in their

review [115]. It is noted that the tendril-like FSAs always need a high temperature to trigger the actuation, which is not safe enough for the wide practical applications.

Apart from the phase change of polymer chains, some FSAs with tendril-shaped structures can be driven by the stress resulting from the inconsistent change in the constituent materials, such as Young's modulus and expansion coefficient. Sim et al. [116] twisted a nylon fiber and then coated a layer of hydrogel on its surface to get a core/shell composite structure. The modulus of hydrogel will decrease during swelling in the phosphate-buffered saline solution. The untwisting force of the core is greater than the recovery force of the sheath. To get a new balanced state, the nylon core tends to recover the original orientation and the composite fiber will transform from the straight shape to the tendril-like shape. When immersed in the solutions with various glucose concentrations, this composite FSA exhibits a reversible tensile stroke as much as 2.3% and the maximum work density arrives at ~ 130 kJ cm^{-3}. Based on the similar mechanism, Li's group [117] cured a layer of epoxy resin on a pre-stretched tendril-shaped CNTs fiber to prepare a composite FSA (Fig. 17b). The epoxy resin can be softened by the electrothermal heating when a voltage is applied on the FSA. The minimum driving voltage is below 0.8 V and the maximum contraction ratio can reach more than 12%. It has also been concluded that the introduction of the tendril-like shape greatly amplifies the thermal-stimulated linear actuation for the bimorph FSA with different thermal expansion abilities [118, 119]. Using a 3D printing technology, Kanik et al. [120] fabricated bimorph FSAs composed of polyethylene and cyclic olefin copolymer elastomer. The bimorph FSAs demonstrate a linear contraction with self-sensing abilities in response to heat or light, and they can lift a load that is more than 650 times their own weight (Fig. 17c). However, there are still some problems for the tendril-like FSAs. For example, there exists a massive room to further enhance the actuation ability of the tendril-like FSAs, including the actuating speed, stroke and stability.

FSA Actuation Based on the Change of Twisted Structures

There are many FSAs with twisted structures as opposed to uniaxial fiber structures. The fibers or yarns used to fabricate these FSAs with twisted structure are anisotropic, and thus they exhibit anisotropic expansion responding to external stimuli. It has been reported that the anisotropic thermal expansion performance plays one key role to trigger the actuation of twisted fibers [121]. Furthermore, the change of the twisted structures always leads to the significant linear stroke combining with a torsion deformation, which is distinct from the actuation behavior of the non-twisted structures.

The yarns or fibers from highly twisted treatment will form a winded coil-like shape to minimize the strain energy. Meanwhile, the twisted treatment also causes an elongation for the fiber along the axial direction [122]. In this case, the actuation direction highly depends on the twisting direction and the winding direction [40]. Generally, the FSAs with a homochirality structure (i.e., the winding direction is consistent with the twisting direction) exhibit a contraction behavior along the fiber axis together with a torsion resulting from the untwisting process. On the contrary, the FSAs with a heterochirality structure (i.e., the winding direction is opposite to the twisting direction) exhibit an elongation behavior during the untwisting process. For instance, Jia et al. [42] reported a self-balanced FSA with twisted silk-fiber structures. When the humidity increases from 20 to 80%, this FSA with the homochirality structure performs

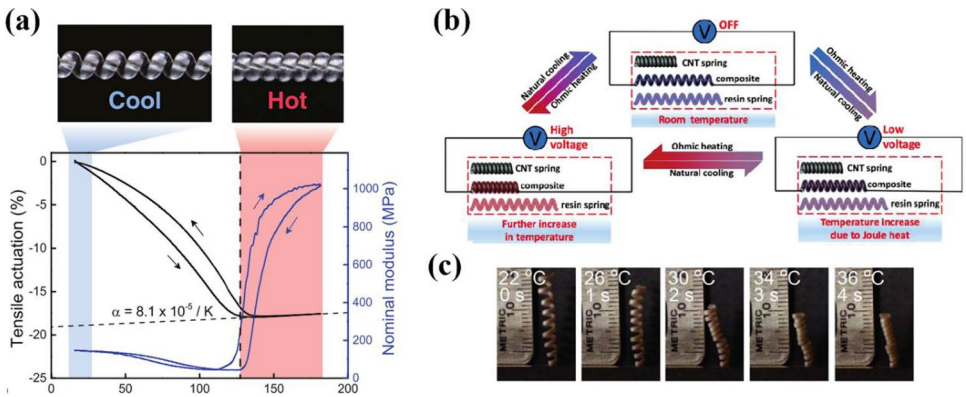

Fig. 17 **a** Digital images of relaxed and contracted fishing line-based FSAs and the corresponding actuation strain change; Reproduced with permission from ref [40], Copyright 2014, AAAS. **b** Schematic illustration of the driving mechanism for the epoxy resin/CNTs FSA; Reproduced with permission from ref [117], Copyright 2019, Royal Society of Chemistry. **c** Contraction behavior of the tendril-like bimorph FSAs in response to a temperature increase; Reproduced with permission from ref [120], Copyright 2019, AAAS

a 47% contraction, while for the heterochirality structure, a 630% extension is available.

In some cases, the change of the twisted structures comes from the change of each individual fiber. This means that the absorption of water or some specific solvents can induce an anisotropic expansion, leading to linear stroke and untwist deformation for the as-twisted FSAs. Wang et al. [21] fabricated an FSA by twisting lotus fiber yarns. Due to plenty of hydrophilic groups in the natural fiber, the FSA has a high sensitivity to the humidity change. When the humidity increases, the yarns expand along the diameter direction and the FSA displays a fully reversible tensile stroke of 38% and the maximum rotation speed of 200 rpm. In addition to the outstanding mechanical strength, the excellent conductivity of CNTs is considered for the design of the FSAs. Peng's group [123] reported an electro-driven CNTs yarn-based FSA. As shown in Fig. 18a, b, once the voltage is applied, an electromagnetic force between the parallel yarns will be induced according to Ampere's Law. As a result, a significant contractive force and a torsional force will be generated simultaneously, which makes the FSA contract and rotate. Importantly, this CNTs yarn-based FSA can be used in diverse environments, including air, water or organic solvent. Furthermore, the voltage applied to drive the actuation is as low as 4 mV and more than 2000 cycles' actuation can be available without any fatigue.

Additionally, the change of twisted structures can be attributed to the change of the materials that are infiltrated or inserted in the space of these twisted fibers. Lima et al. [124] twisted multiwall carbon nanotubes (MWCNTs) yarns and then infiltrated the wax into them to fabricate a composite FSA. Powered by direct heating, applying voltage or the light illumination, the inserted wax can melt, leading to the volume expansion and driving the expansion of the FSA along the radial direction and a contraction along the axial direction. Interestingly, the actuation of the FAS can lift a load over 10 million times of its own weight. Considering the limited thermal-induced expansion and the relative high melting temperature of wax, this group further introduced a solvent-responsive elastomer instead of the wax as the guest material into the twisted MWCNTs fibers. Due to the considerable volume expansion ability (up to 400%), the resulting

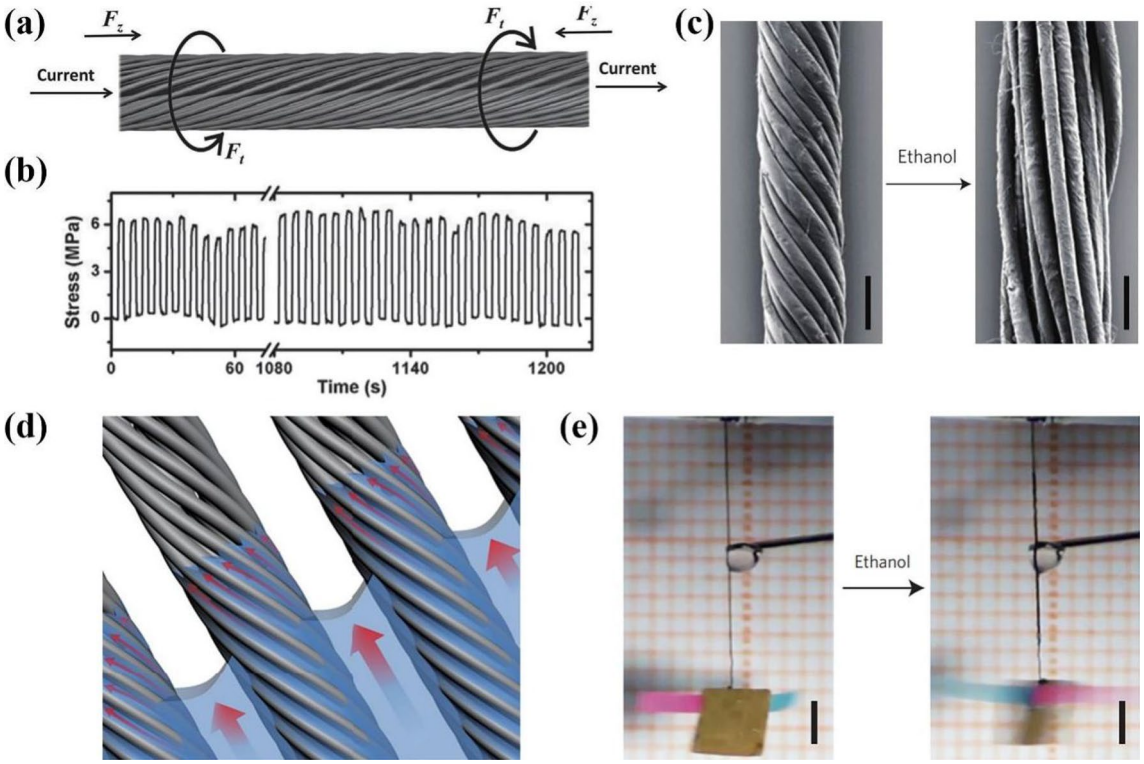

Fig. 18 **a** Schematic illustration of the electromagnetic-driven CNTs yarn-based FSA (F_z: contractive force, F_t: torsional force). **b** Cycle performance of the electromagnetic-driven CNTs yarn-based FSA; Reproduced with permission from ref [123], Copyright 2012, WILEY–VCH. **c** SEM images of the CNT-based FSA with overtwisted structure before and after ethanol infiltration (Scale bar: 40 μm). **d** Schematic illustration of the actuation mechanism of solvent-driven CNT-based FSA with overtwisted structure. **e** Digital photographs of the FSA exposed to ethanol (Scale bar: 2 mm); Reproduced with permission from ref [126], Copyright 2015, Springer Nature

Table 2 Summary of the actuation mechanisms: typical material, structure, and actuation performance

Mechanism	Material	Structure	Performance	Refs.
Fluidic actuation	Soft elastomer	Linear tube	Contraction, elongation	[7], [8], [63], [65–69]
Volume change	Hydrogel	Linear	Torsion, contraction, bending	[60], [74], [78], [79], [83]
Order change	LCP	Linear, twisted	Contraction, torsion, bending	[26], [31], [40], [52], [90], [93], [99], [100], [102], [105], [110–113], [117], [118], [121]
	SMP, SMA	Linear	Contraction	
	DE	Linear	Contraction	
	Nylon, composite materials	Tendril, bimorph tendril	Contraction, torsion	
Change of twisted structure	Natural fiber/yarn, artificial fiber/yarn, CNTs yarn	Twisted structure	Contraction, elongation, torsion	[21], [36], [42], [124–127]

FSA exhibits a reversible contraction of 50% combining with torsion [36]. By substituting MWCNTs for single-wall carbon nanotubes to improve the infiltrating process, Shang et al. [125] realized a more significant reversible contraction of 90% under a relatively lower voltage (2 V). It is noted that the actuation behaviors mentioned above are principally based on the untwisting deformation. Recently, Chen et al. [126] have prepared CNT-based fibers and then twisted them to produce an FSA with helical structures. Their work proves the existence of nanoscale gaps between the aligned nanotubes and micrometer-scale gaps between the primary fibers. When the FSA is exposed to water or polar solvents, the liquid molecules can infiltrate into and enlarge these gaps, inducing a fast contraction together with the torsion deformation. The phenomenon is attributed to the attractive force resulting from the surface tension of liquid, which leads to the further untwisting process of the FSA (i.e., contraction and torsion deformation) (Fig. 18c–e).

As demonstrated above, twisting is a relatively simple method to prepare high-performance FSAs. Furthermore, based on the principle of changing the twisting structure to drive the FSAs, it is very promising to introduce diverse fibrous materials into the FSAs, including natural fibers [21, 22, 42] and artificial fibers [36, 113, 123–125]. No matter whether the raw materials possess the ability of the stimulus-responsive shape change or not, the introduction of twisting structures can enhance the actuation ability of the FSAs. Improving the affinity of the raw fiber or yarn with water or specific solvents is necessary to boost the actuation performances in most cases [42]. Additionally, the FSAs depending on the change of twisted structures usually exhibit a torsion behavior together with the contraction or elongation actuation. It enables the FSAs to be applied in some special conditions where the torsion is regarded as the necessary actuation style.

The above discussion indicates that the actuation mechanism available for the FSAs is intimately related to the used materials and the as-formed structures of the FSAs (Table 2). This provides the basic principle to realize the desirable actuation behavior via the structure design and the composition manipulation of the FSAs.

Applications

Compared to the common soft actuators with 2D plate-shaped structures, the FSAs are more flexible to realize multifunction and adaptability to various devices. So far, the FSAs have demonstrated a promising future in diverse practical applications. In this section, some examples of the applications of the FSAs in recent years will be summarized based on the actuation style and specific structures (Fig. 19).

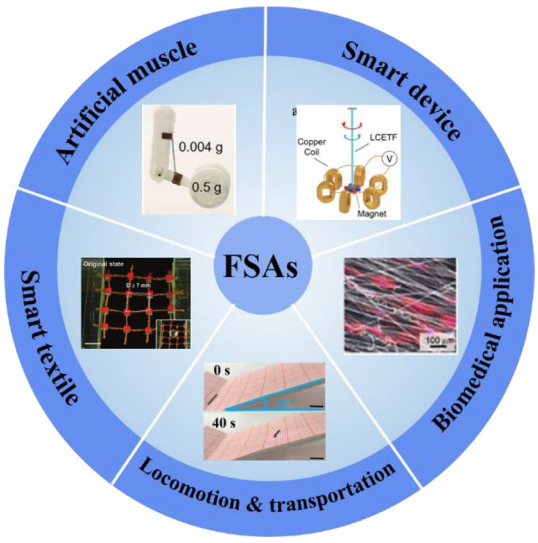

Fig. 19 Summary of the application fields of the FSAs: artificial muscle, smart textile, locomotion and transportation, smart device and biomedical application

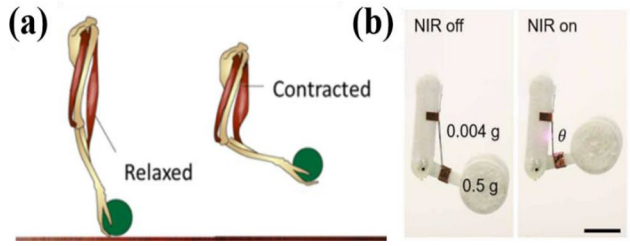

Fig. 20 **a** Schematic illustration of anatomy of a relaxed and contracted bicep muscle fiber; Reproduced with permission from ref [32], Copyright 2019, American Chemical Society. **b** NIR-driven artificial muscle (Scale bar: 10 mm); Reproduced with permission from ref [52], Copyright 2021, AAAS

Artificial Muscle

Stimulated by nervous impulses, muscle fibers exhibit a contraction or relaxation behavior and drive the associated arthrosis to realize specific actions. This is a common life activity for natural lives, especially for the mammal. Most of the reported FSAs can stroke reversibly in response to external stimuli, which is highly similar to the effect of muscles. Hence, the FSAs have been regarded as an ideal candidate for artificial muscles (Fig. 20a). Up to now, a great deal of work focuses on this field [109, 127, 128] to improve the related performances, such as the contraction ratio, response speed, working capacity and mechanical strength. He et al. [52] fabricated an LCE-based FSA by electrospinning and used it as an artificial muscle. The coated polydopamine (PDA) layer makes it easy to remotely control the actuation of the LCE-based FSA with NIR illumination. As shown in Fig. 20b, the FSAs are adapted as a self-made elbow model to stimulate the bicep muscle. This artificial muscle exhibits outstanding performances (e.g., the contraction ratio: above 50%; the contraction stress: 0.3 MPa; the response speed: 300%/s and the volumetric work density: up to 20 kJ m^{-3}), which is comparable to the real muscles. As mentioned above, Mckibben muscle may move more quickly and smoothly to the desired position, which is quite comparable to the real muscles. Mckibben muscle has been applied to design a support suit system and assist people to realize some difficult posture [4]. This kind of FSAs shows the application potential in the bio-robot field. It is pointed out how to control them more accurately is still a problem. As for the practical application in the biomedical field, more attention should be paid to improving the biocompatibility of the employed raw materials and the safety of the control system in living body.

Smart Textile

Smart textile has been emerging in the past several decades. Integrating smart fibers into textile for various functions has aroused increasing attention in the related fields. As for the FSAs, investigators try to use them to endow smart textiles with specific dynamic structures. This kind of dynamic and reversible shape change is driven by the light illumination [26], temperature fluctuation [91], humidity change [21] and so on. For instance, Pang et al. [26] designed a catch net woven-based on a flexible FSA. This FSA is made of azobenzene-based LLCP, which can be driven by UV illumination to perform a significant contraction behavior. Depending on this property, the grid diameter of the obtained woven can be tuned by the simple UV illumination (Fig. 21a). Chen and coworkers used the twisted MWNTs fibers to prepare ethanol-sensitive smart woven. As shown in Fig. 21b, a copper ball is put on a loose woven. When exposed to ethanol, the quick contraction of the woven happens, lifting the ball which is 100 times over its own weight [126]. Weaving FSAs into fabric to prepare smart clothes has been reported in recent years. Owing to the humidity-sensitive ability, the FSAs with twisted structure will contract, triggering a contraction behavior of the as-woven fabric simultaneously. The cloth shortens when people is sweat, and recovers to the initial length when the environment is dry (Fig. 21c). The dynamic change in the shape for the FSA-containing smart textile not only adds the

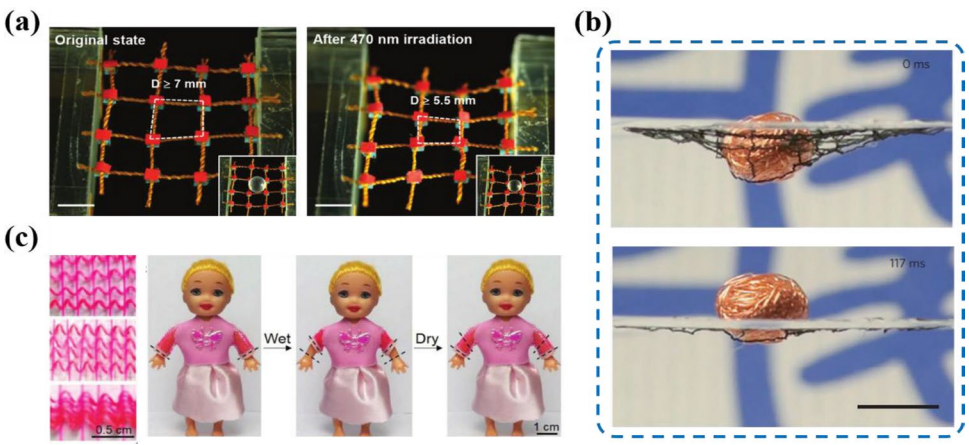

Fig. 21 **a** UV-driven smart textile (Scale bar: 5 mm); Reproduced with permission from ref [26], Copyright 2020, WILEY–VCH. **b** Digital photos of the smart textile lifting a copper ball from ethanol (240 mg). Scale bar: 5 mm; Reproduced with permission from ref [126], Copyright 2015, Springer Nature. **c** Photographs of humidity-sensitive textile and the prepared cloth; Repoduced with permission from ref [42], Copyright 2019, WILEY–VCH

comfortability of the clothes, but also offers the dynamic controllability of special protection materials. Notably, the actuation direction and the actuation stroke of the applied FSAs should be taken into consideration to make the final textile with an ideal deformation as needed. Buckner et al. [105] introduced a ribbon-like FSA into textile to offer the shape change ability. The SMA-based FSA can perform a bending deformation. Hence, the obtained textile can change from 2D to 3D structure according to the program of the inserted FSA. A variety of active textiles are also woven in plain weave using thin McKibben muscle as warps and three types of string as wefts. The contraction ratio and force in the weft direction are related to the pressure applied to McKibben muscle. The contraction properties of active textiles can be altered using various threads as wefts [129].

Locomotion and Transportation

Locomotion and transportation are two kinds of the most common functions for traditional actuators. As for 2D-shaped soft actuators, there exist many restrictions. In the previous studies, most of the locomotions for soft actuators are based on the bending actuation of a "bow-shaped design" [43, 130] or the rolling actuation of a "ring-shaped design" [131]. The actuators with these shape designs can move in a straight line. Meanwhile, a special substrate terrain is always required to assist the locomotion. In the past several years, some investigations have concerned the locomotion of FSAs powered by heating, humidity and light illumination [132–134]. For example, Ahn et al. [134] explored the self-sustained moving of an LCE-based FSA. Illuminated by NIR scattered light or set on a hot plate, the LCE-based FSA will move in a straight line with the moving direction perpendicular to its axis. The LCE-based FSA is further utilized as smart devices for the controlled locomotion and transportation (Fig. 22a). For some FSAs, the moving direction strongly depends not only on the expansion coefficient and the curvature of the fibers [133] (Fig. 22b), but also on the applied stimuli [134]. Recently, a core–shell FSA is prepared by depositing CNTs shell on the LCE fiber [93]. The introduction of CNTs with the excellent photothermal conversion ability endows the resulting FSA with the spatiotemporal modulation of the actuation behavior. Interestingly, the core–shell LCE-based FSA exhibits a phototropic locomotion, including linear moving, climbing and turning in any prescribed direction, while the phototropic locomotion has nothing to do with the precast structure (Fig. 22c). A theoretical modeling has been established to uncover the underlying photo-driven movement mechanism. Owing to the limited weight and size of the FSA, the locomotion stability and transportation load are not as much desirable as people need in daily life. With the in-depth theoretical research, the locomotion of the FSAs will be more and more flexible and steerable. To satisfy the advanced applications, the theoretical model should be adaptable to the devices with larger dimensions and more complex ingenuity.

Smart Device

With the rapid development of our technology level, the emerging smart devices provide a much more convenient and comfortable life. The FSA is one promising candidate for creating smart devices with stimulus-responsive capability because of the excellent actuation performances. For instance, an LCE-based FSA with phototropic bending ability was reported by Lv's group [135]. Depending on this phototropic bending property, the FSA is applied to drive gearwheel rotation. Rotation is a common motion for many

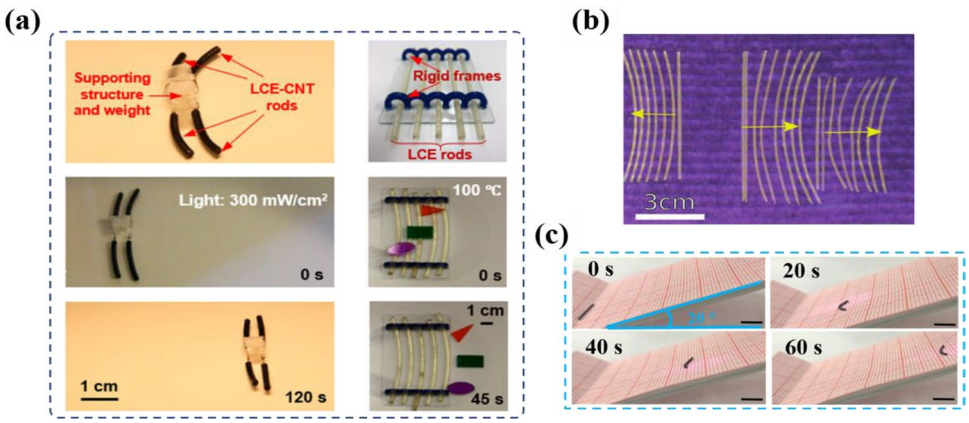

Fig. 22 **a** Photographs of the LCE-based FSA used for the locomotion and transportation; Reproduced with permission from ref [134], Copyright 2018, American Chemical Society. **b** Picture of the humidity-driven locomotion for dry spaghetti; Reproduced with permission from ref [133], Copyright 2020, Royal Society of Chemistry. **c** Phototropic locomotion on a slope surface (Scale bar: 5 mm); Reproduced with permission from ref [93], Copyright 2022, Elsevier

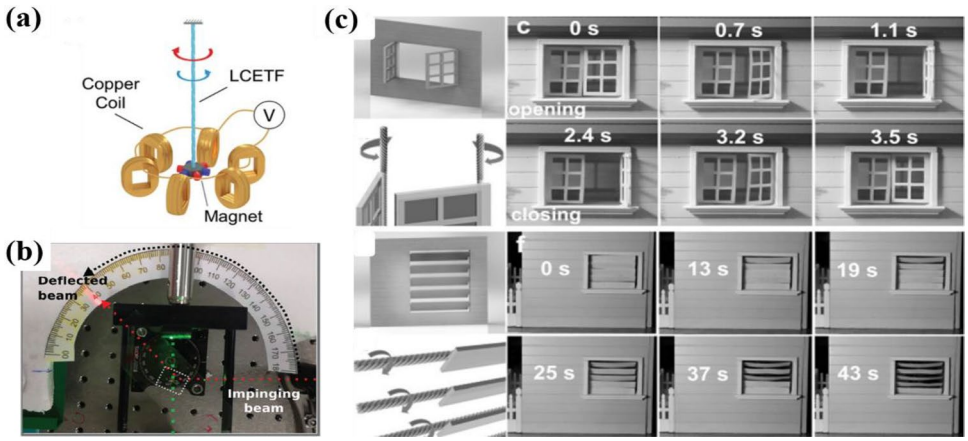

Fig. 23 **a** Schematic illustration of the electricity generator; Reproduced with permission from ref [24], Copyright 2022, WILEY–VCH. **b** Picture of the beam steered by mirror rotation; Reproduced with permission from ref [23], Copyright 2005, Royal Society of Chemistry. **c** Photos of moisture-sensitive shutter; Reproduced with permission from ref [136], Copyright 2015, WILEY–VCH

engineering devices. As mentioned above, the untwisted deformation enables a large number of twisted FSAs to perform this movement. Wang et al. [24] fabricated a soft motor using the LCE-based FSA and connected it with a magnet. Furthermore, a group of copper coils is incorporated with this structure to get an electric generator (Fig. 23a). A mirror is attached at the end of the twisted LCE-based fiber. As a result, the mirror will rotate with the fiber under the external stimulation. This smart device can be used to control the beam path (Fig. 23b) [23]. He et al. [136] proposed a moisture-responsive FSA by twisting CNTs yarns, which can be used as the rotation axis of a shutter. Stimulated by the moisture change, the shutter can be smartly opened or closed within 1.1 s (Fig. 23c). Based on the similar principle, a moisture-driven ventilating device is designed by connecting the baffle with the FSA [20]. When the humidity varies, the baffle will be lifted with the FSA to realize the ventilation. The flexibility of the FSAs makes a positive effect on the miniaturization and portability of smart devices. Moreover, the special powering modes such as the temperature, the moisture and light illumination are different from the normal electric energy. This actually offers many novel ideas to drive smart devices remotely and provides safer working conditions for the operators.

Biomedical Application

As an important issue which is closely related to human living, smart materials used for biomedical applications have been arousing wide attention from various fields. The properties of the controllable dynamic shape change for the FSAs can imitate the dynamic microenvironment change in organism. For example, Niiyama et al. [137] fabricated various nanofiber nets by electrospinning poly(ε-caprolactone)-based polyurethane. The biocompatible materials combined with the oriented nanostructures provide a desirable environment to guide the directional cell culture. Additionally, thanks to the thermal-responsive shape-memory ability, the hybrid nanofiber is highly suitable to control the cell alignment dynamically (Fig. 24a). Namely, the porous nanostructures, the oriented nanofibers and the shape-memory property endow the hybrid nanofibers with wide application

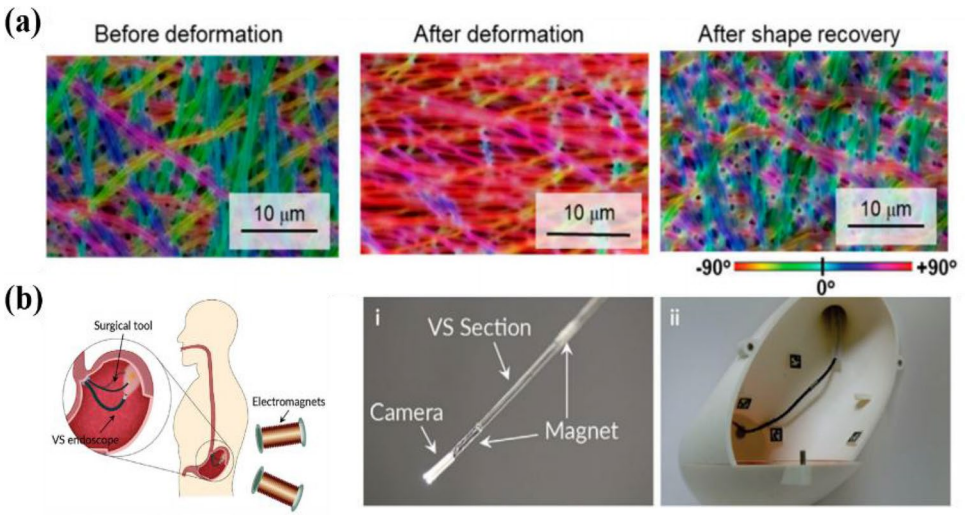

Fig. 24 **a** Orientation analysis of SMP nanofibers before and after the deformation, and after shape recovery; Reproduced with permission from ref [137], Copyright 2019, MDPI. **b** Schematic illustration of an endoscopic procedure performed with a VS endoscope; Reproduced with permission from ref [141], Copyright 2021, WILEY–VCH

potentials in the biomedical field. However, most of the raw materials used in this case always need a relatively higher temperature to trigger the actuation, which makes it difficult to apply in real organisms.

Considering the lower risk and faster recovery time, minimally invasive surgeries are being applied to operate in localized target regions, so as to curtail the damage. One of the most frequently used medical instruments in the operation is a catheter, which is inserted in the body to a specific position for aiding the operation [138]. Recently, increasing interest has been paid to magnetically controlled catheters to achieve more precise movements. Variable stiffness (VS) is seen as an important property to enhance the flexibility of magnetic catheters [139–141]. As shown in Fig. 24b, Bradley and coworkers presented a series of magnetically controlled catheters with VS feature. By adding other functional devices (e.g., camera and surgical tool), these variable stiffness catheters (VSC) can realize more additional functions (Fig. 24b). The good thermal conductivity of these fillers can improve the heat transfer rate. The biocompatible material with a lower T_g, a larger heat transfer rate, and a smaller diameter makes the VSC safer, more flexible, and more controllable [141].

Summary and Perspectives

In this review, the recent progress on the FSAs, including the fabrication, actuation mechanism and applications are summarized. Compared to soft actuators with plate-shaped structures, the FSAs have many internal advantages, such as higher degree of freedom, smaller volume and better adaptability with complex structures [142–144]. However, there are still some challenges to be addressed in the future research. For instance, lots of works have mainly focused on the actual actuation of FSAs experimentally, while the quantitative analysis and theoretical model for some certain actuation of the FSAs still lack. Moreover, different from the traditional actuation driven by electric motor and controlled by electrical system, soft actuators, especially the FSAs, are always driven by the change of external conditions, such as the temperature, the humidity and light illumination. Hence, the lack of stability and accuracy in the change for external conditions will reduce the controllability in the actuation of the FSAs to some extent. Up to now, more and more attention has been paid to realization of more complex and diverse functions of the FSAs [145–147]. However, many works are limited to the fundamental research and theoretical design. More studies are required to promote the FSAs to be closer to the practical applications. Furthermore, with the rapid progress in the material synthesis and material processing technology, it is highly expected that the FSAs with more distinctive functions will be fabricated in large quantities using a much simpler process.

Acknowledgements This work was supported by the National Natural Science Foundation of China (NSFC) (Grant No. 21875160), State Key Laboratory for Modification of Chemical Fibers and Polymer Materials (Grant No. KF2219), JK20202A030463, the Natural Science Foundation of Tianjin City (Grant No. 20JCQNJC00870), and the Scientific Research Project of Tianjin Municipal Education Commission (Grant No. 2020KJ054).

Data availability All data generated or analysed during this study are included in this published article.

Declarations

Conflict of Interest The authors declare no conflict of interest.

References

1. Rus D, Tolley MT. Design, fabrication and control of soft robots. *Nature*. **2015**;*521*:7553.
2. Chen SE, Pang YK, Yuan HY, Tan XB, Cao CY. Smart soft actuators and grippers enabled by self-powered tribo-skins. *Adv Mater Tech*. **2020**;*5*:1901075.
3. Paek J, Cho I, Kim J. Microrobotic tentacles with spiral bending capacity based on shape-engineered elastomeric microtubes. *Sci Rep*. **2015**;*5*:14151.
4. Abe T, Koizumi S, Nabae H, Endo G, Suzumori K. Muscle textile to implement soft suit to shift balancing posture of the body. *IEEE RoboSoft*. **2018**;572–8. https://doi.org/10.1109/ROBOSOFT.2018.8405387.
5. Khodambashi R, Alsaid Y, Rico R, Marvi H, Peet MM, Fisher RE, Berman S, He XM, Aukes DM. Heterogeneous hydrogel structures with spatiotemporal reconfigurability using addressable and tunable voxels. *Adv Mater*. **2021**;*33*:2005906.
6. Le XX, Lu W, Zhang JW, Chen T. Recent progress in biomimetic anisotropic hydrogel actuators. *Adv Sci*. **2019**;*6*:1801584.
7. Hoekstra DC, Debije MG, Schenning APHJ. Triple-shape-memory soft actuators from an interpenetrating network of hybrid liquid crystals. *Macromolecules*. **2021**;*54*:5410–6.
8. Linghu C, Zhang S, Wang CJ, Yu KX, Li CL, Zeng YJ, Zhou HD, Jin XH, You ZY, Song JZ. Universal SMP gripper with massive and selective capabilities for multiscaled, arbitrarily shaped objects. *Sci Adv*. **2020**. https://doi.org/10.1126/sciadv.aay5120.
9. Zhu MM, Wang WJ, Zhang CH, Zhu LP, Yang SG. Photoresponsive behaviors of hydrogen-bonded polymer complex fibers containing azobenzene functional groups. *Adv Fiber Mat*. **2021**;*3*:172–9.
10. Li TF, Li GR, Liang YM, Chen TY, Dai J, Yang XX, Liu BY, Zeng ZD, Huang ZL, Luo YW, Xie T, Yang W. Fast-moving soft electronic fish. *Sci Adv*. **2017**;*3*: e1602045.
11. Ge YH, Cao R, Ye SJ, Chen Z, Zhu ZF, Tu YF, Ge DT, Yang XM. A bio-inspired homogeneous graphene oxide actuator driven by moisture gradients. *Chem Commun*. **2018**;*54*:3126–9.
12. Umrao S, Tabassian R, Kim J, Nguyen VH, Zhou QT, Nam S, Il-Kwon O. MXene artificial muscles based on ionically cross-linked Ti3C2Tx electrode for kinetic soft robotics. *Sci Robot*. **2019**. https://doi.org/10.1126/scirobotics.aaw7797.
13. Wang XQ, Chan KH, Cheng Y, Ding TP, Li TT, Achavananthadith S, Ahmet S, Ho JS, Ghim W. Somatosensory, light-driven,

thin-film robots capable of integrated perception and motility. *Adv Mater*. **2020**;*32*:2000351.
14. Zeng H, Wasylczyk P, Wiersma DS, Priimagi A. Light robots: bridging the gap between microrobotics and photomechanics in soft materials. *Adv Mater*. **2018**;*30*:1703554.
15. Hines L, Petersen K, Sitti M. Inflated soft actuators with reversible stable deformations. *Adv Mater*. **2016**;*28*:3690–6.
16. Lu HF, Wang M, Chen XM, Lin BP, Yang H. Interpenetrating liquid crystal polyurethane/polyacrylate elastomer with ultrastrong mechanical property. *J Am Chem Soc*. **2019**;*36*:14364–9.
17. Yang Y, Pei Z, Li Z, Wei Y, Ji Y. Making and remaking dynamic 3d structures by shining light on flat liquid crystalline vitrimer films without a mold. *J Am Chem Soc*. **2016**;*138*:2118–21.
18. Verpaalen RCP, Da CMP, Engels TAP, Debije MG, Schenning APHJ. Liquid crystal networks on thermoplastics: reprogrammable photo-responsive actuators. *Angew Chem Int Ed*. **2020**;*59*:4532–6.
19. Bombara D, Fowzer S, Zhang J. Compliant, large-strain, and self-sensing twisted string actuators. *Soft Robot*. **2022**;*9*:1.
20. Kim SH, Kwon CH, Park K, Mun TJ, Lepro X, Baughman RH, Spinks GM, Kim SJ. Bio-inspired, moisture-powered hybrid carbon nanotube yarn muscles. *Sci Rep*. **2016**;*6*:23016.
21. Wang Y, Wang Z, Lu ZY, Jung DAM, Fang SL, Zhang ZQ, Wu JP. Baughman RH Humidity- and water-responsive torsional and contractile lotus fiber yarn artificial muscles. *ACS Appl Mater*. **2021**;*13*:6642.
22. Yang XH, Wang WH, Miao MH. Moisture-responsive natural fiber coil-structured artificial muscles. *ACS Appl Mater*. **2018**;*10*:32256.
23. Nocentini S, Martella D, Wiersma DS, Parmeggiani C. Beam steering by liquid crystal elastomer fibres. *Soft Matter*. **2017**;*13*:8590.
24. Wang Y, Sun J, Liao W, Yang ZQ. Liquid crystal elastomer twist fibers towards rotating microengines. *Adv Mater*. **2021**;*34*:2107840.
25. Lv JA, Liu Y, Wei J, Chen EQ, Qin L, Yu YL. Photocontrol of fluid slugs in liquid crystal polymer microactuators. *Nature*. **2016**;*537*:179.
26. Pang X, Qin L, Xu B, Liu Q, Yu YL. Ultralarge contraction directed by light-driven unlocking of prestored strain energy in linear liquid crystal polymer fibers. *Adv Funct Mater*. **2020**;*30*:2002451.
27. An YM, Gao LM, Wang TY. Graphene oxide/alginate hydrogel fibers with hierarchically arranged helical structures for soft actuator application. *ACS Appl Nano Mater*. **2020**;*3*:5079.
28. Omura T, Komiyama K, Maehara A, Kabe T, Iwata T. Elastic marine biodegradable fibers produced from poly (r)-3-hydroxybutylate-co-4-hydroxybutylate and evaluation of their biodegradability. *ACS Appl Polym Mater*. **2021**;*3*:6479.
29. Sharma K, Braun O, Tritsch S, et al. 2D Raman, ATR-FTIR, WAXD, SAXS and DSC data of PET mono-and PET/PA6 bicomponent filaments. *Data Brief*. **2021**;*38*: 107416.
30. Wang L, Zhang MY, Yang B, Tan JJ. Lightweight, robust, conductive composite fibers based on mxene@aramid nanofibers as sensors for smart fabrics. *ACS Appl Mater*. **2021**;*13*:41933.
31. Qi X, Yang W, Yu L, Wang WJ, Wu YL, Zhu SW, Zhu YF, Liu XD, Dong YB, Fu YQ. Design of ethylene-vinyl acetate copolymer fiber with two-way shape memory effect. *Polyms Basel*. **2019**;*11*:1599.
32. Roach DJ, Yuan C, Kuang X, Li VCF, Blake P, Romero ML, Hammel I, Yu K, Qi HJ. Long liquid crystal elastomer fibers with large reversible actuation strains for smart textiles and artificial muscles. *ACS Appl Mater Interfaces*. **2019**;*11*:19514.
33. Uh K, Yoon B, Lee CW, Kim JM. An electrolyte-free conducting polymer actuator that displays electrothermal bending and flapping wing motions under a magnetic field. *ACS Appl Mater Interfaces*. **2016**;*8*:1289–96.
34. Lin XY, Saed MO, Terentjev EM. Continuous spinning aligned liquid crystal elastomer fibers with a 3D printer setup. *Soft Matter*. **2021**;*17*:5436.
35. Lin S, Wang Z, Chen XY, Ren J, Ling SJ. Ultrastrong and highly sensitive fiber microactuators constructed by force-reeled silks. *Adv Sci*. **2020**;*7*:1902743.
36. Lima MD, Hussain MW, Spinks GM, Naficy S, Hagenasr D, Bykova JS, Tolly D, Baughman RH. Efficient, absorption-powered artificial muscles based on carbon nanotube hybrid yarns. *Small*. **2015**;*11*:3113.
37. Yuan JK, Neri W, Zakri C, Merzeau P, Kratz K, Lendlein A, Poulin P. Shape memory nanocomposite fibers for untethered high-energy microengines. *Science*. **2019**;*365*:155.
38. Koziol K, Vilatela J, Moisala A, Moisala A, Motta M, Cunniff P, Snnett M, Windle A. High-performance carbon nanotube fiber. *Science*. **2007**;*318*:1892.
39. Lee DM, Park J, Lee J, Lee SH, Kim SH, Kim SM, Jeong SH. Improving mechanical and physical properties of ultra-thick carbon nanotube fiber by fast swelling and stretching process. *Carbon*. **2021**;*172*:733.
40. Haines CS, Lima MD, Li N, Spinks GM, Foroughi J, Madden JDW, Kim SH, Fang SL, Jung DAM, Goktepe F, Goktepe O, Mirvakili SM, Naficy S, Lepro XJ, Koziov ME, Kim SJ, Xu XR, Swedlove BJ, Wallace GG, Baughman RH. Artificial muscles from fishing line and sewing thread. *Science*. **2014**;*343*:868.
41. Liu ZS, Zhang R, Xiao YC, Li JT, Chang W, Qian D, Liu ZF. Somatosensitive film soft crawling robots driven by artificial muscle for load carrying and multi-terrain locomotion. *Mater Horizons*. **2021**;*8*:1783.
42. Jia TJ, Wang Y, Dou YY, Li YW, Andrade MJD, Wang R, Fang SL, Li JJ, Yu Z, Qiao R, Liu ZJ, Cheng Y, Su YW, Minary-Jolandan M, Baughman RH, Qian D, Liu ZF. Moisture sensitive smart yarns and textiles from self-balanced silk fiber muscles. *Adv Funct Mater*. **2019**;*29*:1808241.
43. Xue J, Wu T, Dai Y, Xia YN. Electrospinning and electrospun nanofibers: methods, materials, and applications. *Chem Rev*. **2019**;*119*:5298.
44. Wu JL, Hong Y. Enhancing cell infiltration of electrospun fibrous scaffolds in tissue regeneration. *Bioactive Mater*. **2016**;*1*:56.
45. Han ZP, Wang JQ, Liu SP, Liu YJ, Luo SY, Guo F, Ma JY, Li P, Ming X, Chao G, Zhen X, Zhang QH, Tan YQ. Electrospinning of neat graphene nanofibers. *Adv Fiber Mater*. **2022**;*4*:268.
46. Li CP, Qiu M, Li RL, Li X, Wang MX, He JB, Qiang QR, Chen QH, Li XY, Chen YM, Qiu M, Xiao LR, Lin GG, Wu JX, Mai YW. Electrospinning engineering enables high-performance sodium-ion batteries. *Adv Fiber Mater*. **2022**;*4*:43.
47. Yin J, Ahmed A, Xu L. High-Throughput free surface electrospinning using solution reservoirs with different depths and its preparation mechanism study. *Adv Fiber Mater*. **2021**;*3*:251.
48. Xue JJ, Xie JW, Liu WY, Xia YN. Electrospun nanofibers: new concepts, materials, and applications. *Acc Chem Res*. **2017**;*50*:1976.
49. Cha DI, Kim YH, Lee KH, Jung YC, Cho JW, Chun BC. Electrospun nonwovens of shape-memory polyurethane block copolymers. *J Appl Polym Sci*. **2005**;*96*:460.
50. Wang L, Zhang F, Liu Y, Leng JS. Shape memory polymer fibers: materials, structures, and applications. *Adv Fiber Mater*. **2022**;*4*:5.
51. Zhuo HT, Hu JL, Chen SJ. Study of the thermal properties of shape memory polyurethane nanofibrous nonwoven. *J Mater Sci*. **2011**;*46*:3464.
52. He Q, Wang Z, Wang Y, Wang ZJ, Li CH, Annapooranan R, Zeng J, Chen RK, Cai SQ. Electrospun liquid crystal elastomer

microfiber actuator. *Sci Robot*. **2021**. https://doi.org/10.1126/scirobotics.abi9704.
53. Jeong W, Kim J, Kim S, Lee S, Mensing G, Beebe DJ. Hydrodynamic microfabrication via "on the fly" photopolymerization of microscale fibers and tubes. *Lab Chip*. **2004**;*4*:576.
54. Du XY, Li Q, Wu G, Chen S. Multifunctional micro/nanoscale fibers based on microfluidic spinning technology. *Adv Mater*. **2019**;*31*:1903733.
55. Li Q, Xu Z, Du XY, Cheng HY, Wu G, Wang CF, Cui ZF, Chen S. Microfluidic-directed hydrogel fabrics based on interfibrillar self-healing effects. *Chem Mater*. **2018**;*30*:8822.
56. Lim D, Lee E, Kim H, Park S, Beak S, Yoon J. Multi stimuli-responsive hydrogel microfibers containing magnetite nanoparticles prepared using microcapillary devices. *Soft Matter*. **2015**;*11*:1606.
57. Stannarius R, Eremin A, Harth K, Morys M, DeMiglio A, Ohm C, Zentel R. Mechanical and optical properties of continuously spun fibres of a main-chain smectic A elastomer. *Soft Matter*. **1858**;*2012*:8.
58. Tang MJ, Wang W, Li ZL, Guo ZY, Tian HY, Liu Z, Ju XJ, Xie R, Chu LY. Controllable microfluidic fabrication of magnetic hybrid microswimmers with hollow helical structures. *Ind Eng Chem Res*. **2018**;*57*:9430.
59. Kotikian A, Morales JM, Lu A, Mueller J, Davidson Z, Boley JW, Lewis JA. Innervated, self-sensing liquid crystal elastomer actuators with closed loop control. *Adv Mater*. **2021**;*33*:2101814.
60. Duan XY, Yu JY, Zhu YX, Zheng ZQ, Liao QH, Xiao YK, Li YY, He ZP, Zhao Y, Wang HP, Qiu LT. Large-scale spinning approach to engineering knittable hydrogel fiber for soft robots. *ACS Nano*. **2020**;*14*:14929.
61. Naciri J, Srinivasan A, Jeon H, Nikolov N, Keller P, Ratna BR. Nematic elastomer fiber actuator. *Macromolecules*. **2003**;*36*:8499.
62. Yuk H, Lin ST, Ma C, Takaffoli M, Fang NX, Zhao XH. Hydraulic hydrogel actuators and robots optically and sonically camouflaged in water. *Nat Commun*. **2017**;*8*:14230.
63. Grellmann H, Lohse FM, Kamble VG, Winger H, Nocke A, Hickmann R, Wiessner S, Cherif C. Fundamentals and working mechanisms of artificial muscles with textile application in the loop. *Smart Mater Struct*. **2022**;*31*: 023001.
64. Giri N, Walker I. Continuum robots and underactuated grasping. *Mech Sci*. **2011**;*2*:51.
65. Kurumaya S, Nabae H, Endo G, Suzumori K. Active textile braided in three strands with thin McKibben muscle. *Soft Robot*. **2019**;*6*:2.
66. Cacucciolo V, Nabae H, Suzumori K, Shea H. Electrically-driven soft fluidic actuators combining stretchable pumps with thin Mckibben muscles. *Front Robot AI*. **2020**;*6*:146.
67. Cacucciolo V, Shintake J, Kuwajima Y, Maeda S, Floreano D, Shea H. Stretchable pumps for soft machines. *Nature*. **2019**;*572*:516.
68. Daerden F, Lefeber D, Verrelst B, Han Van R. Pleated pneumatic artificial muscles: compliant robotic actuators. *Proceedings 2001 IEEE/RSJ IROS.* **2001**, *4*: 1958.
69. Li ST, Zhang R, Zhang GH, Shuai LYZ, Chang W, Hu XY, Zou M, Zhou X, An BG, Qian D, Liu ZF. Microfluidic manipulation by spiral hollow-fibre actuators. *Nat Commun*. **2022**;*13*:1331.
70. Ilmain F, Tanaka T, Kokufuta E. Volume transition in a gel driven by hydrogen bonding. *Nature*. **1991**;*349*:400.
71. Suzuki A, Tanaka T. Phase-transition in polymer gels induced by visible-light. *Nature*. **1990**;*346*:345.
72. Tanaka T, Fillmore D, Sun ST, Nishio I, Swislow G, Shah A. Phase transitions in ionic gels. *Phys Rev Lett*. **1980**;*45*:1636.
73. Li X, Cai XB, Gao YF, Serpe MJ. Reversible bidirectional bending of hydrogel-based bilayer actuators. *J Mater Chem B*. **2017**;*5*:2804.
74. Liu XY, Xu H, Zhang LQ, Zhong M, Xie XM. Homogeneous and real super tough multi-bond network hydrogels created through a controllable metal ion permeation strategy. *ACS Appl Mater*. **2019**;*11*:42856.
75. Warren DS, Sutherland SPH, Kao JY, Weal GR, Mackay SM. The preparation and simple analysis of a clay nanoparticle composite hydrogel. *J Chem Educ*. **2017**;*94*:1772.
76. Li L, Shan H, Yue CY, Lam YC, Tam KC, Hu X. Thermally induced association and dissociation of methylcellulose in aqueous solutions. *Langmur*. **2002**;*20*:7291.
77. Southall NT, Dill KA, Haymet ADJ. A view of the hydrophobic effect. *J Phys Chem B*. **2002**;*10*:2812.
78. Jalani G, Jung CW, Lee JS, Lim DW. Fabrication and characterization of anisotropic nanofiber scaffolds for advanced drug delivery systems. *Int J Nanomed*. **2014**;*9*:33.
79. You CW, Qin WJ, Yan Z, Ren ZX, Huang JY, Ii JT, Chang W, He WQ, Wen K, Yin SG, Zhou X, Liu ZF. Highly improved water tolerance of hydrogel fibers with a carbon nanotube sheath for rotational, contractile and elongational actuation. *J Mater Chem A*. **2021**;*9*:10240.
80. Terasawa N, Takeuchi I, Matsumoto H. Electrochemical properties and actuation mechanisms of actuators using carbon nanotube-ionic liquid gel. *Sensor Actuat B: Chem*. **2009**;*139*:624.
81. Terasawa N, Takeuchi I. Electrochemical property and actuation mechanism of an actuator using three different electrode and same electrolyte in air: Carbon nanotube/ionic liquid/polymer gel electrode, carbon nanotube/ionic liquid gel electrode and Au paste as an electrode. *Sensor Actuat B Chem*. **2010**;*145*:775.
82. Wang YH, Bian K, Hu CG, Zhang ZP, Chen N, Zhang HM, Qu LT. Flexible and wearable graphene/polypyrrole fibers towards multifunctional actuator applications. *Electrochem Commun*. **2013**;*35*:49.
83. Zheng J, Xiao P, Le XX, Lu W, Theao P, Ma CX, Du BY, Zhang JW, Huang YJ, Chen T. Mimosa inspired bilayer hydrogel actuator functioning in multi-environments. *J Mater Chem C*. **2018**;*6*:1320.
84. Vorlander D. Investigation of the molecular form by means of crystalline liquids. *Z Phys Chem*. **1923**;*105*:211.
85. Jackson WJ, Kuhfuss HF. Liquid crystal polymers. I. Preparation and properties ofp-hydroxybenzoic acid copolyesters. *J Polym Sci Part A Polym Chem*. **1996**;*34*:3031–55.
86. Ube T, Ikeda T. Photomobile polymer materials with complex 3D deformation, continuous motions, self-regulation, and enhanced processability. *Adv Opt Mater*. **2019**;*7*:1900380.
87. Qing X, Lv JA, Yu YL. Photodeformable liquid crystal polymers. *Acta Polym Sin*. **2017**;*11*:1679.
88. White TJ, Broer DJ. Programmable and adaptive mechanics with liquid crystal polymer networks and elastomers. *Nat Mater*. **2015**;*14*:1087.
89. Ge FJ, Zhao Y. Microstructured actuation of liquid crystal polymer networks. *Adv Funct Mater*. **2020**;*30*:1901890.
90. Cheng ZX, Ma SD, Zhang YH, Huang S, Chen YX, Yu HF. Photomechanical motion of liquid-crystalline fibers bending away from a light source. *Macromolecules*. **2017**;*50*:8317.
91. Lan R, Sun J, Shen C, Huang R, Zhang ZP, Zhang LY, Wang L, Yang H. Near-infrared photodriven self-sustained oscillation of liquid-crystalline network film with predesignated polydopamine coating. *Adv Mater*. **2020**;*32*:1906319.
92. Wang Y, Dang A, Zhang Z, Yin R, Gao YC, Feng L, Yang S. Repeatable and reprogrammable shape morphing from photoresponsive gold nanorod/liquid crystal elastomers. *Adv Mater*. **2020**;*32*:2004270.

93. Yu Y, Li LL, Liu EP, Han X, Wang JJ, Xie YX, Lu CH. Light-driven core-shell fiber actuator based on carbon nanotubes/liquid crystal elastomer for artificial muscle and phototropic locomotion. *Carbon*. **2022**;*187*:97.
94. Dong L, Zhao Y. Photothermally driven liquid crystal polymer actuators. *Mater Chem Front*. **1932**;*2018*:2.
95. Orozco F, Kaveh M, Santosa DS, Lima GMR, Gomes DR, Pei YT, Araya-Hermosilla R, Moreno-Villoslada I, Picchioni F, Bose RK. Electroactive self-healing shape memory polymer composites based on diels-alder chemistry. *ACS Appl Polym Mater*. **2021**;*3*:6147.
96. Sun WJ, Guan Y, Wang YY, Wang T, Xu YT, Kong WW, Jia LC, Yan DX, Li ZM. Low-voltage actuator with bilayer structure for various biomimetic locomotions. *ACS Appl Mater Interfaces*. **2021**;*13*:43449.
97. Zhang L, Lin ZH, Zhou Q, Ma SQ, Liang YH, Zhang ZH. PEEK modified PLA shape memory blends: towards enhanced mechanical and deformation properties. *Front Mater Sci*. **2020**;*2*:177.
98. Voit W, Ware T, Dasari RR, Smith P, Danz L, Simon D, Barlow S, Marder SR, Gall K. High-strain shape-memory polymers. *Adv Funct Mater*. **2010**;*20*:162.
99. Qi XM, Dong YB, Islam MZ, Zhu YF, Fu YQ, Fu SY. Excellent triple-shape memory effect and superior recovery stress of ethylene-vinyl acetate copolymer fiber. *Compos Sci Technol*. **2021**;*203*: 108609.
100. Lang C, Lloyd EC, Matuszewski KE, Xu YF, Ganesan V, Huang R, Kumar M, Hickey RJ. Nanostructured block copolymer muscles. *Nat Nanotec*. **2022**;*17*:752.
101. Khoury LR, Popa I. Chemical unfolding of protein domains induces shape change in programmed protein hydrogels. *Nat Commun*. **2019**;*10*:5439.
102. Cera L, Gonzalez GM, Liu QH, Choi S, Chantre CO, Lee J, Gabardi R, Choi MC, Shin K, Parker KK. A bioinspired and hierarchically structured shape-memory material. *Nat Mater*. **2021**;*20*:242.
103. Wang J, Zhao QL, Cui HQ, Wang YL, Chen HX, Du XM. Tunable shape memory polymer mold for multiple microarray replications. *J Mater Chem A*. **2018**;*6*:24748.
104. Cui CH, An L, Zhang ZL, Ji MK, Chen K, Yang YX, Su Q, Wang F, Cheng YL, Zhang YF. Reconfigurable 4D printing of reprocessable and mechanically strong polythiourethane covalent adaptable networks. *Adv Funct Mater*. **2022**;*32*:2203720.
105. Buckner TL, Bilodeau RA, Kim SY, Kramer-Bottiglio R. Roboticizing fabric by integrating functional fibers. *PNAS*. **2021**;*117*:25360.
106. Brochu P, Pei QB. Advances in dielectric elastomers for actuators and artificial muscles. *Macromol Rapid Commun*. **2010**;*31*:10.
107. Pelrine R, Kornbluh R, Pei QB, Joseph J. High-speed electrically actuated elastomers with strain greater than 100%. *Science*. **2000**;*287*:836.
108. Qiu Y, Zhang E, Plamthottam R, Pei QB. Dielectric elastomer artificial muscle: materials innovations and device explorations. *Acc Chem Res*. **2019**;*52*:316.
109. Mirvakili SM, Hunter IW. Artificial muscles: mechanisms, applications, and challenges. *Adv Mater*. **2018**;*30*:1704407.
110. Kofod G, Stoyanov H, Gerhard R. Multilayer coaxial fiber dielectric elastomers for actuation and sensing. *Appl Phys A*. **2011**;*102*:577.
111. Arora S, Ghosh T, Muth J. Dielectric elastomer based prototype fiber actuators. *Sens Actuat-A Phys*. **2007**;*1*:321.
112. Shimizu K, Nagai T, Shintake J. Dielectric elastomer fiber actuators with aqueous electrode. *Polymers*. **2021**;*13*:4310.
113. Chortos A, Mao J, Mueller J, Hajiesmaili E, Lewis JA, Clarke DR. Printing reconfigurable bundles of dielectric elastomer fibers. *Adv Funct Mater*. **2021**;*31*:2010643.
114. Wan GC, Jin CR, Trase I, Zhao S, Chen Z. Helical structures mimicking chiral seedpod opening and tendril coiling. *Sensors*. **2018**;*18*:2973.
115. Haines CS, Li N, Spinks GM, Aliev AE, Di JT, Baughman RH. New twist on artificial muscles. *PNAS*. **2016**;*113*:11709.
116. Sim HJ, Jang Y, Kim H, Choi JG, Park JW, Lee DY, Kim SJ. Self-helical fiber for glucose-responsive artificial muscle. *ACS Appl Mater Inerfaces*. **2020**;*12*:20228.
117. Xu LL, Peng QY, Zhu Y, Zhao X, Yang MD, Wang SS, Xue FH, Yuan Y, Lin ZS, Xu F, Sun XX, Li JJ, Yin WL, Li YB, He XD. Artificial muscle with reversible and controllable deformation based on stiffness-variable carbon nanotube spring-like nanocomposite yarn. *Nanoscale*. **2019**;*11*:8124.
118. Amjadi M, Sitti M. High-performance multiresponsive paper actuators. *ACS Nano*. **2016**;*10*:10202.
119. Lu C, Park S, Richner TJ, Derry A, Brown I, Hou C, Rao SY, Kang J, Moritz CT, Fink Y, Anikeeva P. Flexible and stretchable nanowire-coated fibers for optoelectronic probing of spinal cord circuits. *Sci Adv*. **2017**;*3*: e1600955.
120. Kanik M, Orguc S, Varnavides G, Kim J, Benavides T, Gonzalez D, Akintilo T, Tasan CC, Chandrakasan AP, Fink Y, Anikeeva P. Strain-programmable fiber-based artificial muscle. *Science*. **2019**;*365*:145.
121. Kimura D, Irisawa T, Takagi K, Tahara K, Sakurai D, Watanabe H, Takarada W, Shioya M. Mechanism for anisotropic thermal expansion of polyamide fibers. *Sensor Actuat B Chem*. **2021**;*344*: 130262.
122. Ghatak A, Mahadevan L. Solenoids and plectonemes in stretched and twisted elastomeric filaments. *Phys Rev Lett*. **2005**;*95*: 057801.
123. Guo WH, Liu C, Zhao FY, Sun XM, Yang ZB, Chen T, Chen XL, Qiu LB, Hu XH, Peng HS. A Novel Electromechanical actuation mechanism of a carbon nanotube fiber. *Adv Mater*. **2012**;*24*:5379.
124. Lima MD, Li N, De Andrade MJ, Fang SL, Oh J, Spinks GM, Kozlov ME, Haines CS, Suh D, Foroughi J, Kim SJ, Chen YS, Ware T, Shin MK, Machado LD, Fonseca AF, Madden JD, Voit WE, Gavao DS, Baughman RH. Electrically, chemically, and photonically powered torsional and tensile actuation of hybrid carbon nanotube yarn muscles. *Science*. **2012**;*338*:928.
125. Shang YY, He XD, Wang CH, Zhu LY, Peng QY, Shi EZ, Wu ST, Yang YB, Xu WJ, Wang RG, Du SY, Cao AY, Li YB. Large-deformation, multifunctional artificial muscles based on single-walled carbon nanotube yarns. *Adv Eng Mater*. **2015**;*17*:14.
126. Chen PN, Xu YF, He SS, Sun XM, Pan SW, Deng J, Chen DY, Peng HS. Hierarchically arranged helical fibre actuators driven by solvents and vapours. *Nat Nanotech*. **2015**;*10*:1077.
127. Choi K, Park SJ, Won M, Park CH. Soft fabric muscle based on thin diameter SMA springs. *Smart Mater Struct*. **2022**;*31*: 055020.
128. Nishimura Y, Spinks GM. Detailing the visco-elastic origin of thermo-mechanical training of twisted and coiled polymer fiber artificial muscles. *J Polym Sci*. **2022**;*60*:1360.
129. Hiramitsu T, Suzumori K, Nabae H, Endo G. Experimental evaluation of textile mechanisms made of artificial muscles. *IEEE RoboSoft*. **2019**;1–6. https://doi.org/10.1109/ROBOSOFT.2019.8722802.
130. Shahsavan H, Aghakhani A, Zeng H, Guo YB, Davidson ZS, Priimagi A, Sitti M. Bioinspired underwater locomotion of light-driven liquid crystal gels. *PNAS*. **2020**;*117*:5125.
131. Xiang SL, Su YX, Yin H, Li C, Zhu MQ. Visible-light-driven isotropic hydrogels as anisotropic underwater actuators. *Nano Energy*. **2021**;*85*: 105965.

132. Baumann A, Sánchez-Ferrer A, Jacomine L, Martinoty P, Houerou VL, Ziebert F, Kulic IM. Motorizing fibres with geometric zero-energy modes. *Nat Mater*. **2018**;*17*:523.
133. Bazir A, Baumann A, Ziebert F, Kulic IM. Dynamics of fiberboids. *Soft Matter*. **2020**;*16*:5210.
134. Ahn C, Li K, Cai SQ. Light or thermally-powered autonomous rolling of an elastomer rod. *ACS Appl Mater Interfaces*. **2018**;*10*:25689.
135. Hu ZM, Li YL, Zhao TH, Lv JA. Self-winding liquid crystal elastomer fiber actuators with high degree of freedom and tunable actuation. *Appl Mater Today*. **2022**;*27*:101449.
136. He SS, Chen PN, Qiu LB, Wang BJ, Sun XM, Xu YF, Peng HS. A mechanically actuating carbon-nanotube fiber in response to water and moisture. *Angew Chem Int Ed*. **2015**;*54*:14880.
137. Niiyama E, Tanabe K, Uto K, Kikuchi A, Ebara M. Shape-memory nanofiber meshes with programmable cell orientation. *Fibers*. **2019**;*7*:20.
138. Fischer C, Boehler Q, Nelson BJ. Using magnetic fields to navigate and simultaneously localize catheters in endoluminal environments. *IEEE Robot Autom Lett*. **2022**;*3*:7217.
139. Piskarev Y, Shintake J, Chautems C, Lussi J, Boehler Q, Nelson BJ, Floreano D. A variable stiffness magnetic catheter made of a conductive phase-change polymer for minimally invasive surgery. *Adv Funct Mater*. **2022**;*20*:2107662.
140. Lussi J, Mattmann M, Sevim S, Grigis F, De Marco C, Chautems C, Pane S, Puigmart-Luis J, Boehler Q, Nelson BJ. A submillimeter continuous variable stiffness catheter for compliance control. *Adv Sci*. **2021**;*18*:2101290.
141. Mattmann M, De Marco C, Briatico F, Tagliabue S, Colusso A, Chen XZ, Lussi J, Chautems C, Pane S, Nelson B. Thermoset shape memory polymer variable stiffness 4D robotic catheters. *Adv Sci*. **2021**;*1*:2103277.
142. Wang WJ, Xu X, Zhang CH, Huang H, Zhu LP, Yue K, Zhu MF, Yang SG. Skeletal muscle fibers inspired polymeric actuator by assembly of triblock polymers. *Adv Sci*. **2022**;*9*:2105764.
143. Liu DZ, Zhu LP, Huang WT, Yue K, Yang SG. Polymer complex fiber for linear actuation with high working density and stable catch-state. *ACS Macro Lett*. **2020**;*9*:1507–13.
144. Zhu MM, Wang WJ, Zhang CH, Zhu LP, Yang SG. Photoresponsive behaviors of hydrogen-bonded polymer complex fibers containing azobenzene functional groups. *Adv Fiber Mater*. **2021**;*3*:172–9.
145. Zuo XW, Fan TT, Qu LJ, Zhang XJ, Miao JL. Smart multi-responsive aramid aerogel fiber enabled self-powered fabrics. *J Mater Chem C*. **2022**;*10*:14027–52.
146. Li JF, Sun JX, Wu D, Huang WT, Zhu MF, Reichmanis E, Yang SG. Functionalization-directed stabilization of hydrogen-bonded polymer complex fibers: elasticity and conductivity. *Adv Fiber Mater*. **2019**;*1*:71–81.
147. Zhu LP, Yang SG, Zhu MF. Fibers make a better life. *Chin J Polym Sci*. **2022**;*40*:331–2.

Yue Yu obtained a Bachelor of Materials Science and Engineering from Tiangong University (TGU) in 2019. She obtained her Master's degree in the field of materials engineering from Tianjin University (TJU), China. Currently, she is focusing on functional flexible composites and their applications.

Juanjuan Wang is a lecturer in the School of Materials Science and Engineering at Tianjin Chengjian University, China. She obtained her PhD degree in the field of materials at Tianjin University in 2019. From 2017 to 2018, she was a visiting student at Leibniz Institute of Polymer Research Dresden supported by CSC. Her research interests are focused on smart materials and structures, including stimulus-responsive polymers, smart surfaces with nano/microstructures and their applications.

Xue Han is a lecturer in the School of Materials Science and Engineering at Tianjin Chengjian University, China. She obtained her PhD degree in the School of Materials Science and Engineering at Tianjin University, China. Her research interests are focusing on some functional materials, including photoluminescent materials, photochromic materials, electrochromic materials and their applications. She has authored or co-authored over 10 scientific papers.

Shuguang Yang received his BS in 2002 at Wuhan University and his PhD in 2007 at the Institute of Chemistry, Chinese Academy of Sciences. After research assistant at Peking University and a postdoc at The University of Akron, he joined Donghua University (DHU) and was appointed as a full professor of the College of Materials Science and Engineering. He has served as Associate Director of the Center for Advanced Low-dimension Materials (CALM) since 2016. He published 130

peer-reviewed research papers, and his research interests involve polymer complex, fluoropolymer, adaptive fibers, and separation membrane.

Gaihong An is an Assistant Professor in the Environmental and Operational Medicine Research Department at Military Medical Sciences Academy, China. She mainly engaged in special environment operational ability assessment and maintenance improvement technology research, and participated in and undertook over 20 national and military research projects. She has authored or co-authored over 50 scientific papers in different journals and took out more than 10 national invention patents and software copyrights.

Conghua Lu is a full professor at the School of Materials Science and Engineering at Tianjin Chengjian University. Prof. Lu obtained his Bachelor's degree in Polymer Materials and Engineering from the Beijing Institute of Technology in 1996 and his PhD in Polymer Science and Engineering from Peking University in 2003. After two years postdoctoral research in the department of Physical Chemistry of Peking University, he carried out his postdoctoral research at the Max Planck Institute of Colloids and Interfaces in Germany supported by Humboldt Research Fellowships. In 2008, he joined the School of Material Science and Engineering at Tianjin University as a full professor. In 2020, he worked in the School of Materials Science and Engineering at Tianjin Chengjian University. He has published 90 peer-reviewed research papers. His research interests mainly involve smart materials/structures/systems, micro/nanofabrication, and functional materials surface/interface.